5th of 5 files

Chapters 7 and 8
Appendix and References

EFFECT OF STRESS ON INITIATION AND PROPAGATION OF LOCALIZED CORROSION IN ALUMINIUM ALLOYS

By

SUKANTA GHOSH

A thesis submitted to
University of Birmingham
for the degree of
DOCTOR OF PHILOSOPHY

Metallurgy and Materials
School of Engineering
University of Birmingham

November 2007

7 X-RAY SYNCHROTRON TOMOGRAPHIC STUDY OF LOCALIZED CORROSION PROPAGATION IN ALUMINIUM ALLOYS

X-ray synchrotron tomography is a relatively new non-destructive technique which has found ever increasing use in various fields of materials science and engineering for acquiring three dimensional (3D) information of materials. New generation synchrotron sources are able to deliver reconstruction of three dimensional images with spatial resolution close to 1 μm. Because of the resolution in the micron or sub micron level, X-ray synchrotron tomography is sometime referred as X-ray synchrotron microtomography. Basic theory of x-ray synchrotron tomography and its advantages over conventional two-dimensional techniques has been discussed in Section 2.4 (Chapter 2) and can also be found elsewhere [261-267]. Details of the experimental set up for performing X-ray synchrotron experiments can be found in Chapter 3. X-ray microtomography can overcome the limitations of 2D techniques (e.g. true size distribution and connectivity of phases with complex shapes) and provides information about what happens in the bulk material [268]. Reconstruction of the 3D volumetric data from this technique allows for the analysis of the microstructure, defects, phase distribution or damage in the bulk material along with the ability to view two dimensional cross sections at any particular plane or orientation in a non-destructive manner.

The key purpose of this present study is to examine the effect of stress on growth and development of localized corrosion (i.e., intergranular corrosion) in a high strength aluminium alloy. Aerospace aluminium alloy AA2024 in a sensitised temper condition was used for this study. AA2024 specimens were heat treated for 2 hours at 250˚C

followed by water quenching. This particular heat treatment had shown to simulate the electrochemical behaviour of the heat affected zone (HAZ) in the friction stir welded plate [70]. Details of the heat treatment can be found in Chapter 3 and further synchrotron experiments with this particular sensitized temper in unstressed condition is reported elsewhere [235, 288]. Yield strength (Y.S.) of the heat treated AA2024 was determined to be approximately 375 MPa. Experiments were performed on both unstressed and stressed (70% Y.S. and 90% Y.S.) samples.

The evolution of intergranular corrosion (IGC) in aluminium alloys is a problem of fundamental interest to the corrosion community for several years and also somewhat poorly understood. So far only 2D techniques have been used for growth rate quantifications. However, because of the limitations of the conventional two dimensional techniques it is difficult to measure a 3D phenomena such as IGC evolution inside the bulk alloys. So, in this study, high resolution in situ X-ray synchrotron microtomography has been used to record the three dimensional evolution of localized corrosion sites in an aqueous chloride solution, as a function of applied stress and exposure time. Outcome of this work will provide quantitative growth rates of intergranular corrosion and thereby significantly contribute to the ongoing modelling effort for life prediction of aircraft components.

7.1 Two Dimensional Visualization of Localized Corrosion Morphology

Figure 7.1a and b shows the examples of two reconstructed X-ray tomographic slices from a single plane of an unstressed and stressed (90% Y.S.) bulk AA2024

sensitized specimens after exposure of 15 h and 22.4 h, respectively. These reconstructed images (i.e., Figure 7.1a-b) are obtained from the in situ exposure in 0.6 M NaCl solution during the synchrotron experiments. Several features of the bulk alloy can be revealed from these tomographs[30] without actually destroying the specimen. As these tomographs are generated using absorption mode[31], different atomic number of different elements inside the bulk alloy creates contrast in the tomographs helping to provide good visualization of intermetallic particles and intergranular corrosion sites. It can be seen from Figure 7.1(a) that the higher atomic number intermetallic particles appear bright in the microstructure. These intermetallic particles sometimes appear as a band aligning parallel to the rolling direction.

As the specimens are made from a rolled plate, three different directions are assigned to each of the samples, longitudinal (L), transverse (T) and short transverse (S).[32] Figure 7.2 shows the schematic of a typical specimen with these three different orientations. It can be seen that the longer side of the specimen is in the transverse (T) direction. Stressed samples were subjected to load in the transverse (T) direction. Figure 7.2 also schematically explains how a single slice from a single plane is represented within the bulk specimen. Figure 7.1(a) and (b) show that the attacks are intergranular (IGC) in nature and normally follow the L direction which is also the rolling direction. Pre-existing cavities (predominantly associated with the intermetallic particles) within the bulk alloy can also be easily identified from these tomographs.

[30] A tomograph is a 2D slice or plane within the 3D reconstructed X-ray attenuation data.

[31] Different modes of X-ray synchrotron tomography is described in Chapter 3.

[32] Procedure of making ‘matchstick’ cylindrical specimen and dog-bone specimen from the rolled AA2024 plate is described in Chapter 3.

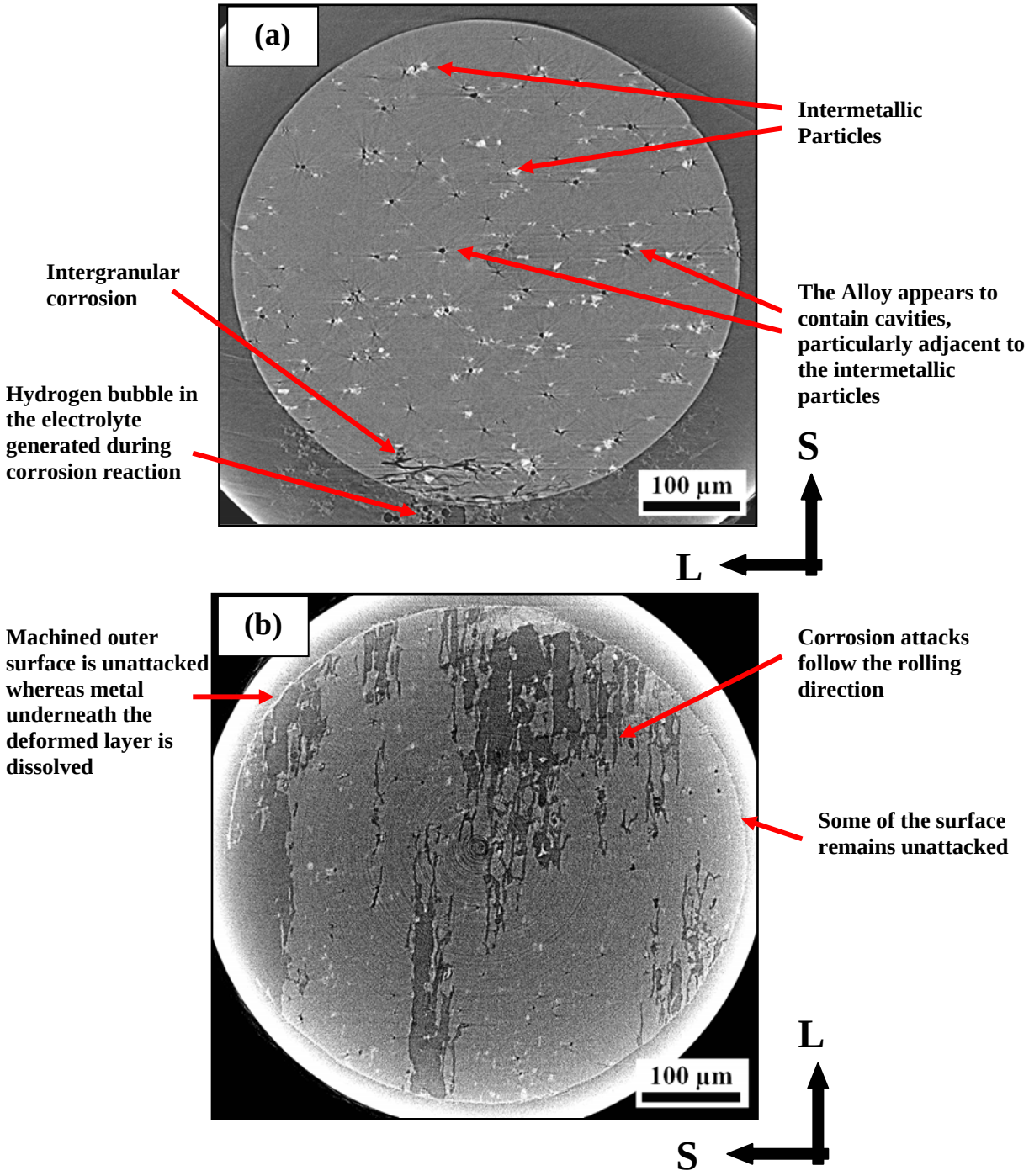

Figure 7.1 Reconstructed tomographic slice of a single plane through the sensitized AA2024 specimen (i.e., heat treated at 250˚C for 2h) after in situ open circuit exposure in 0.6 M NaCl, (a) Unstressed, after 15 h exposure and (b) Samples stressed to 90% YS, after 22.4 h exposure. L = Longitudinal Direction, S = Short Transverse Direction.

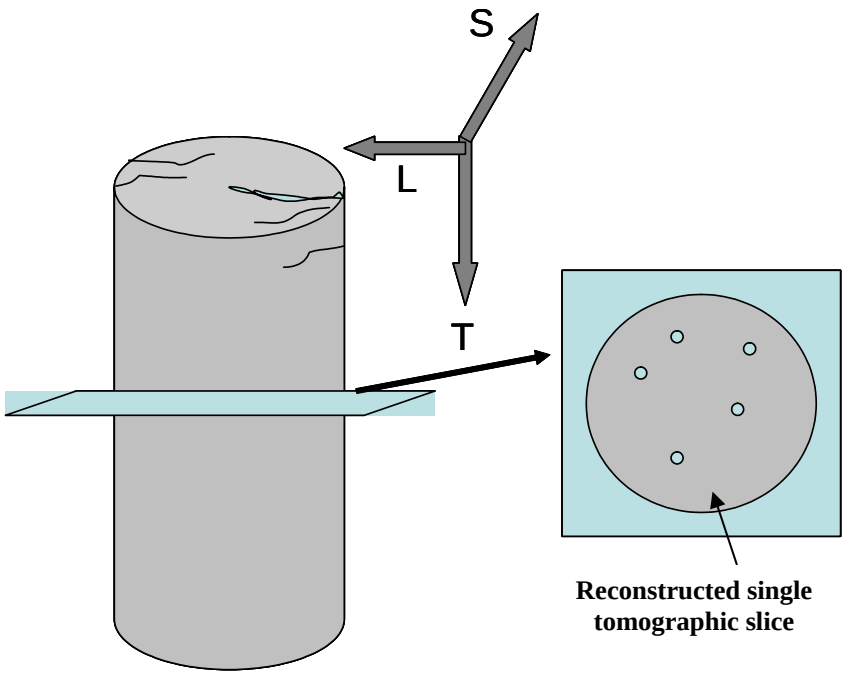

Figure 7.2 Schematic of a typical experimental specimen of sensitized AA2024 sample with different orientations. L = Longitudinal Direction, S = Short Transverse Direction, and T = Transverse Direction. Stress is applied in the transverse (T) direction. It should be noted that for unstressed condition cylindrical matchstick specimen and under stressing condition dog-bone shaped specimens were used. However, in both cases specimen orientations are represented in the way represented in the schematic.

It is interesting to note that all intermetallic particles are not attacked and results in IGC (see Figure 7.1a). This is evident from the fact that in many cases intermetallic particle remain unattacked on the alloy surface. Hydrogen bubbles can also be seen in the solution surrounding the specimen. These hydrogen bubbles are generated from the supporting cathodic reaction during the corrosion process.

Figure 7.1b shows extensive IGC attacks of the sensitized AA2024 specimen stressed to 90% Y.S after 22.4 h of exposure. During the later stages of the localized corrosion event, the evolution of the IGC is associated with considerable amount of grain interior dissolution and/or fallout of grains. One interesting observation in this tomographic slice is that, at some places of the sample surface, the corrosion rate seems

lower than that of the bulk of the material. These differential corrosion rates in two adjacent areas result in considerable undercutting of the specimen. This may be an indication that the machining process for manufacturing the specimens can actually affect the corrosion susceptibility and the rate of local attacks on the surface [288].

Progressive development and coalescence of localized corrosion sites within the bulk of unstressed and stressed AA2024 specimens (in a sensitized temper condition) have been studied through in situ X-ray tomographic scans of individual specimens at four different times during continuous exposure in naturally aerated 0.6 M NaCl solution. Tomographic scans as a function of exposure time not only help to quantify the rate and mode of intergranular attack, but it also gives the opportunity to visualize any possible interaction between the constituent particles and propagating localized corrosion attacks.

Tomographic images of the interaction between a growing IGC site with an intermetallic particle within the bulk of an unstressed AA2024 specimen as a function of exposure time is shown in Figure 7.3. It is interesting to note that IGC initiated adjacent to an intermetallic near the outer surface of the specimen. However, it should also be remembered that IGC does not always initiate near all of the intermetallic particles exposed to the sample surface. These observations re-emphasize the fact that localized corrosion initiation in a material is a stochastic process [18]. Large (size range 10-30 μm) and irregular shaped intermetallic particles in AA2024 are identified as Fe-Mn particles which act as cathodic sites (i.e., provide better surface for cathodic reaction) during the corrosion process.[33] Hence some intermetallic particles remain unattacked even after 34 h of exposure in 0.6 M NaCl (Figure 7.3d). Intergranular corrosion around the intermetallic particle grows without affecting the particle. Dissolution of the surrounding

[33] Morphology and corrosion properties of different intermetallic particles present in AA2024 is described in details in Chapter 4 and 5.

alloy matrix can easily be seen. IGC sites propagate in the L direction and simultaneous widening of the localized corrosion site occurs. Gradual widening of two adjacent intergranular corrosion sites due to grain dissolution result into coalescence of corrosion sites. Hydrogen bubbles adjacent to the corroding alloy [Figure 7.3b, c and d] results from the supporting cathodic reaction.

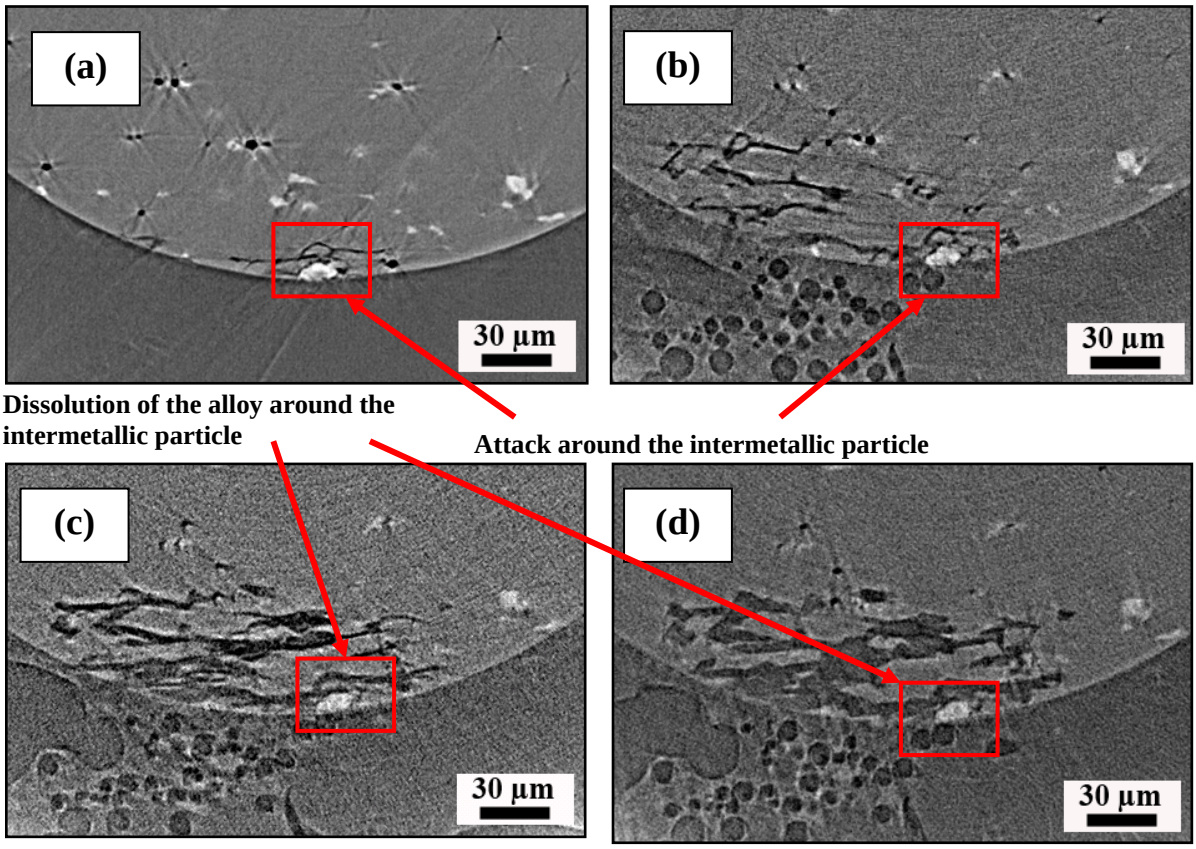

Figure 7.3 A series of reconstructed tomographic slices of a particular plane through the sensitized AA2024 specimen (i.e., heat treated at 250˚C for 2h) in unstressed condition after in situ open circuit exposure in 0.6 M NaCl for (a) 3.4 h , (b) 15 h, (c) 25.6 h, and (d) 33.9 h. These tomographs illustrate the interaction between a propagating intergranular attack and intermetallic particles.

Localized corrosion evolution at a particular site in a single plane of tomographic slices of an unstressed cylindrical AA2024 sample (sensitised tempered) is shown in

Figure 7.4. Series of these exposures prove that localized corrosion does not initiate in or adjacent to all exposed constituent particles. Even after 34 h of exposure in 0.6 M NaCl solution new corrosion sites did not develop. IGC initiated only at a single site and propagated as can be seen from the tomographic images (Figure 7.4). Normally it is found that initially IGC attack follows the longer grain paths in the rolling direction (L). IGC growth in L direction and broadening of those localized corrosion sites occur simultaneously during the exposure. However, intergranular attack stops growing in the L direction after 25 h of immersion (Figure 7.4c) and starts widening at a faster rate which may be caused by grain dissolution and/or grain fall out. Hydrogen bubbles associated with the corrosion of aluminium can be seen at the site of localized corrosion. Fox [235] performed both ex situ study of simulated HAZ and in situ study of a HAZ of a friction stir welded AA2024-T3 in aerated 0.6M NaCl under open circuit condition. Results from Fox's study also emphasized that localized corrosion does not necessarily initiate at all constitute particle and after a certain amount of growth, IGC stops growing (or grows at a much reduced rate) in the L direction but continues to corrode locally via subsequent and considerable grain loss/or fall out adjacent to the IGC sites.

Figure 7.5 shows 2D tomographs of reconstructed X-ray attenuation data of IGC evolution at a particular site in a single plane in the sensitized tempered AA2024 sample stressed to 70% of its yield strength (YS). Two predominant sites are found to be evolving as a function of time, one in the top left corner and second one in the bottom of the images shown in Figure 7.5. Growth of the top left IGC attack is found to cease (or significantly decrease) in the L direction after 16.9 h. This observation is quite similar to that found in unstressed sample.

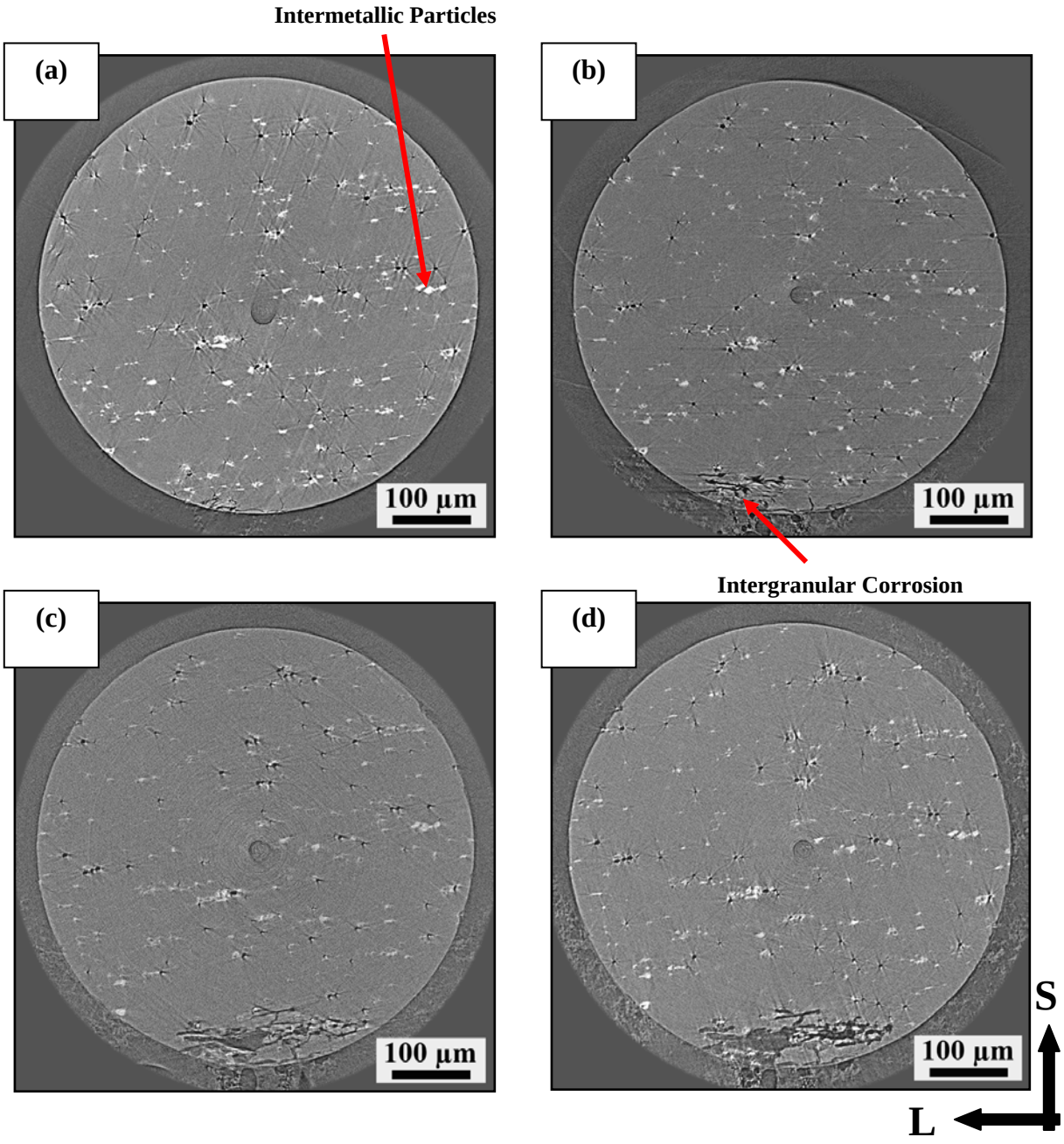

Figure 7.4 Reconstructed 2D tomographic images showing the evolution of IGC at a particular site in the sensitized AA2024 specimen (i.e., heat treated at 250˚C for 2h) in unstressed condition after in situ open circuit exposure in 0.6 M NaCl as a function of time, i.e., (a) 3.4 h, (b) 15 h, (c) 25.6 h, and (d) 33.9 h of exposure. [Hydrogen bubble resulting from the supporting cathodic reaction on the specimen can be seen in each tomograph]. L = Longitudinal direction which is also rolling direction, S = Short Transverse Direction.

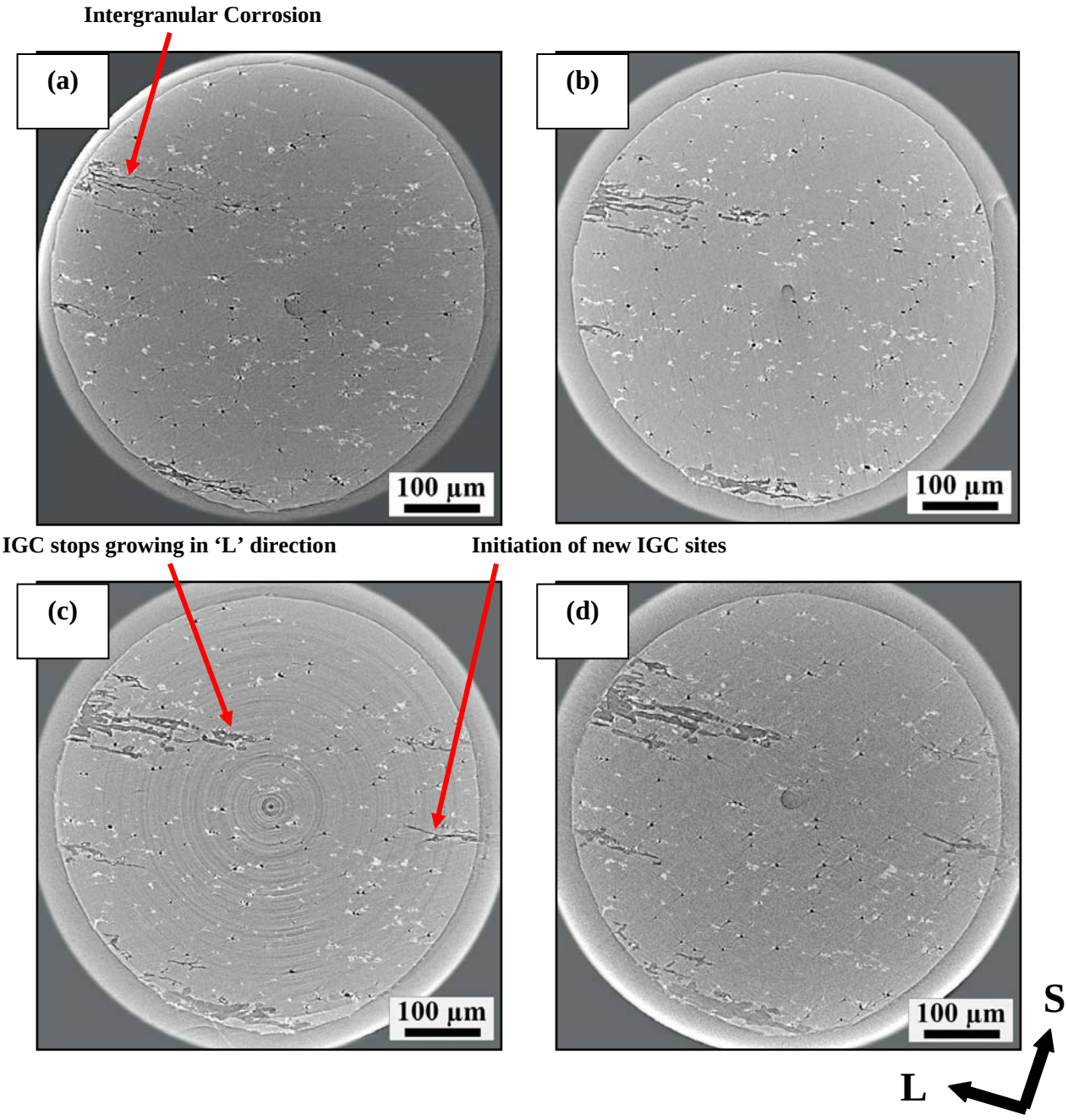

Figure 7.5 Reconstructed 2D tomographic images showing the evolution of IGC at a particular site in the sensitized (i.e., heat treated at 250˚C for 2h) and stressed (70% yield strength) AA2024 specimen after in situ open circuit exposure in 0.6 M NaCl as a function of time, i.e., (a) 5.6 h, (b) 16.9 h, (c) 27.6 h, and (d) 35.9 h of exposure. IGC stops growing in 'L' direction after certain time and new IGC sites initiates (c). L = Longitudinal direction which is also rolling direction, S = Short Transverse Direction. Stress is applied in transverse direction, T.

The IGC network at the bottom of the tomographic slices has virtually penetrated through bulk of the sample and reached the other exterior surface of the specimen within the first six hours of exposure (Figure 7.5c). Another corrosion site (which could be new or may just be growing in the T direction in 3D) appears after 27.6 h in the middle right side of Figure 7.5c. As seen in unstressed samples, IGC in stressed sample also stops growing in L direction and broadening of IGC sites occur through grain interior dissolution and/or grain fall out.

Volume analysis in three dimensions (3D) showed an increase in volume loss as a function of time which proves that, though IGC stop growing (or significantly decreases growth rate) in the L direction it continues to grow in other directions. It may be possible that in both stressed and unstressed samples in many cases localized corrosion initiates as pitting attacks which later develop as intergranular corrosion.

Figure 7.6 shows the tomographs at a particular site in a single plane of the AA2024 sample stressed to 90% of its yield strength as a function of exposure time in 0.6 M NaCl. A significant amount of attacks have been observed after 10.9 h of exposure (Figure 7.6a) and after 22.4 h of exposure propagating IGC sites start widening via dissolution of the grain interior adjacent to the IGC sites. It is interesting to note that (Figure 7.6c), though the outer surface of the sample is still intact in some portions, significant IGC occurred underneath the surface. This undercutting suggests that there are some areas on the surface of the specimen where the corrosion rate is lower than the bulk of the material. One possible explanation for this undercutting is that the machining operation for manufacturing those specimens possibly has an effect on the corrosion susceptibility and local rate of attack on the surface [288].

Effect of applied stress on the intergranular corrosion of heat treated AA2024 specimens can be visualized from three representative tomographs of three different samples shown in Figure 7.7. All samples were exposed in 0.6 M NaCl under open circuit corrosion conditions. The tomograph of the unstressed sample (Figure 7.7a) represent corrosion at a particular plane within the specimen after 15 hours of exposure, where as 70% Y.S. (Figure 7.7b) and 90% Y.S. (Figure 7.7c) tomographs are after 17 h and 11 h of exposure respectively. It should be noted that though tomographic images of three different samples with three different exposure times are compared in this figure, the effect of stress is quite prominent. More IGC attacks can be seen in the sample stressed to 90% Y.S. even with shorter exposure time than the unstressed or 70% Y.S. specimens.

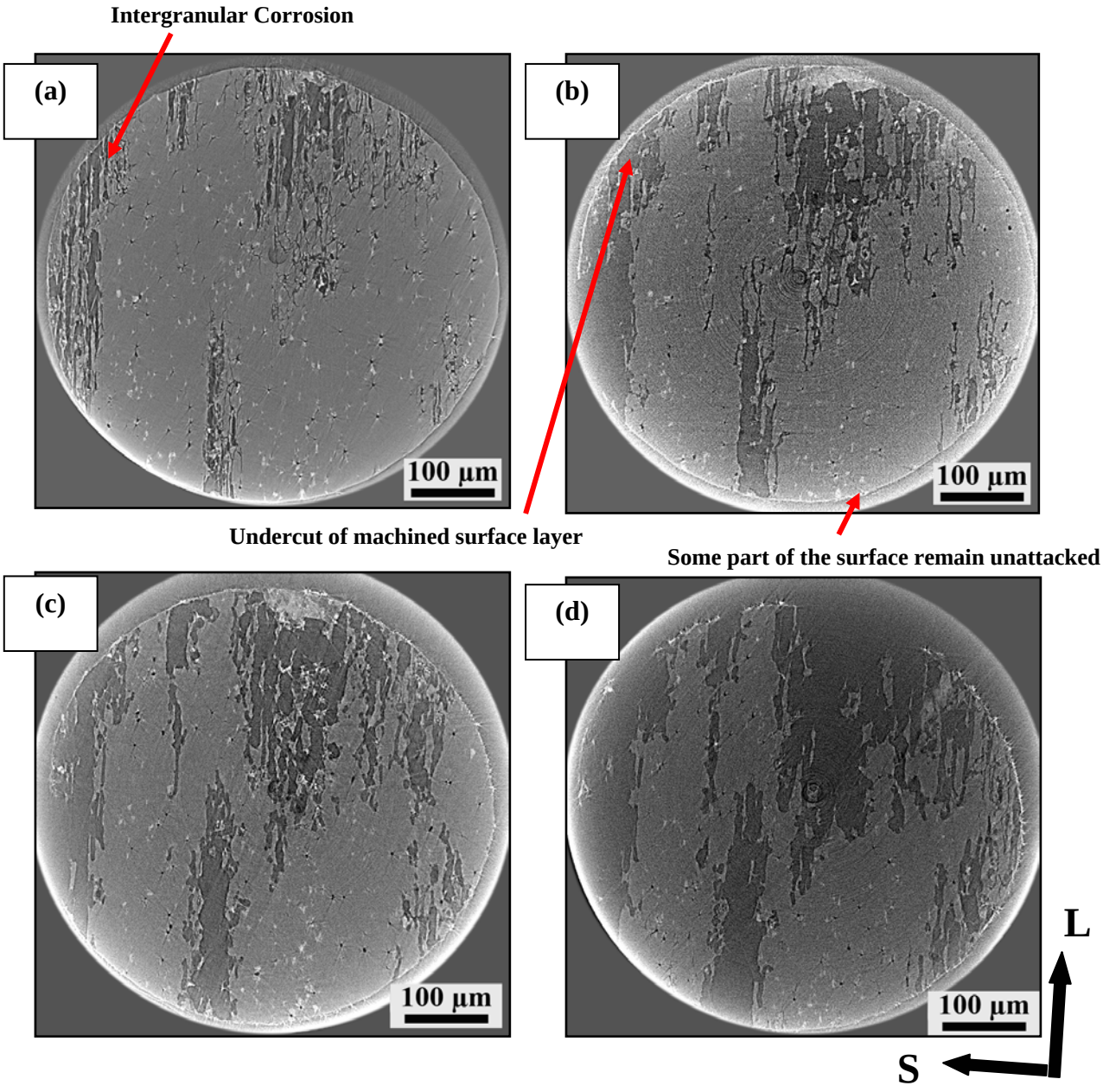

Figure 7.6 Reconstructed 2D tomographic images showing the evolution of IGC at a particular site in the sensitized (i.e., heat treated at 250˚C for 2h) and stressed (90% yield strength) AA2024 specimen after in situ open circuit exposure in 0.6 M NaCl as a function of time, i.e., (a) 10.9 h, (b) 22.4 h, (c) 33.2 h, and (d) 41.2 h of exposure. Severe corrosion attacks can be seen after 22 h of immersion, though some portions of the surface remain unattacked. L = Longitudinal direction which is also rolling direction, S = Short Transverse Direction. Stress is applied in transverse direction, T.

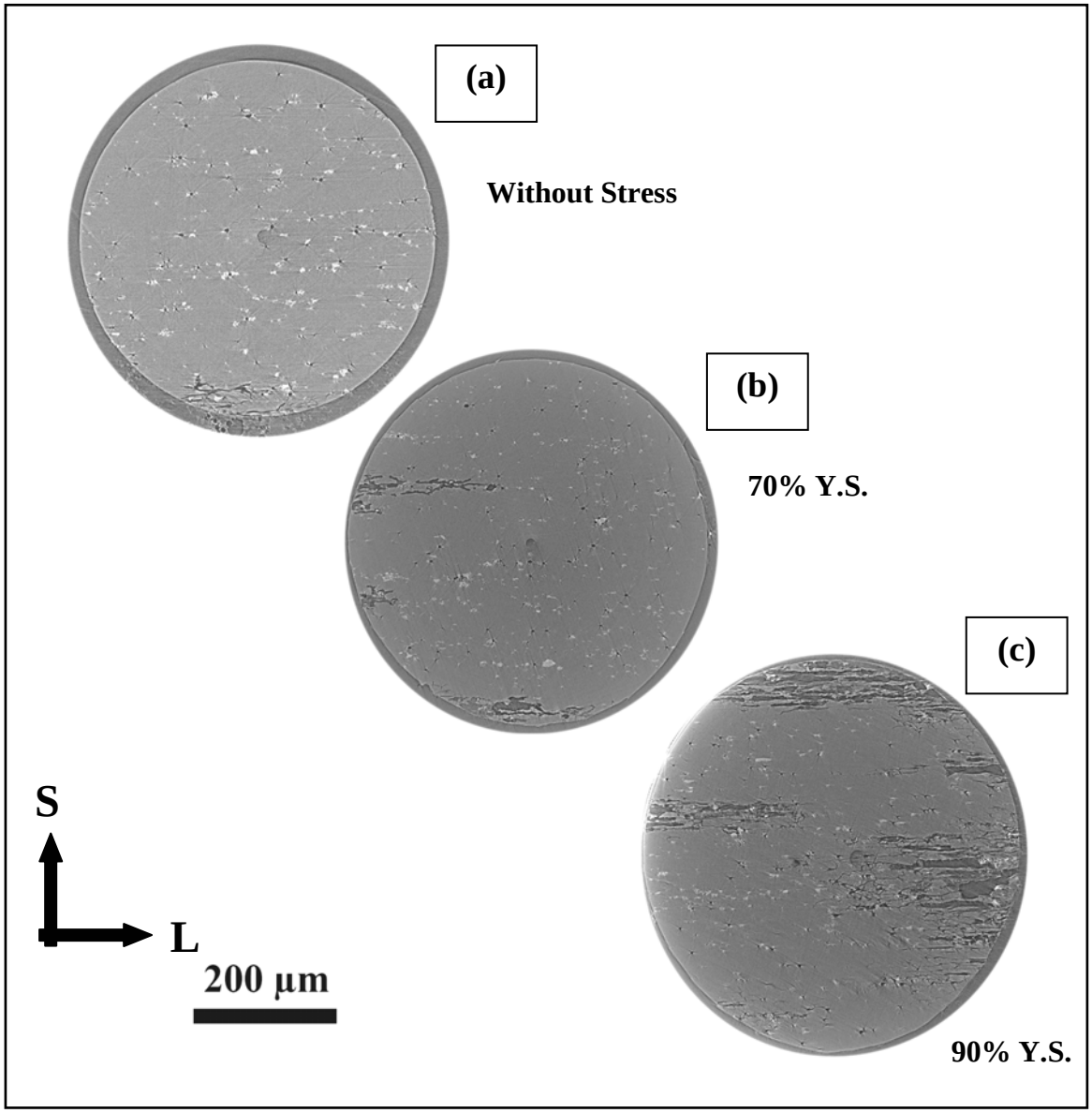

Figure 7.7 Reconstructed 2D tomographic images showing the effect of stress on the intergranular corrosion evolution in sensitized (i.e., heat treated at 250˚C for 2h) AA2024 specimens after in situ open circuit exposure in 0.6 M NaCl, (a) Unstressed sample after 15 h of exposure, (b) Sample stressed to 70% Y.S. after 16.9 h of exposure, and (c) Sample stressed to 90% Y.S. after 10.9 h of exposure. It should be noted that though tomographic images of three different samples with different exposure time are compared in this figure, effect of stress is prominent. More IGC attacks have been seen in 90% YS sample even with shorter exposure time than the other two specimens. L = Longitudinal direction which is also rolling direction, S = Short Transverse Direction. Stress is applied in transverse direction, T.

7.2 Three Dimensional Visualization of Localized Corrosion Morphology

Two dimensional tomographs can be combined together in a stack to provide a 3D representation of the IGC morphology and its interaction with the alloy microstructure.[34] Figure 7.8 shows such 3D rendering of the tomographic data for ~ 150 slices of corroded areas from different samples. Top and side views of these 3D images confirm the intergranular nature of the attack without any presence of cracking. Specimen matrix material has been rendered translucent in order to observe the intergranular attacks which are labelled in green within the interior of the specimen.

It is clearly visible from Figure 7.8 that localized corrosion attacks are following the grain boundaries of the elongated grains in the rolling direction. Several localized corrosion sites initiate along the exposed section of the specimen (T direction) and grow in the L direction in parallel (refer back to Figure 7.2 for orientation details in a specimen). Several of these localized corrosion sites coalesce and form a plate like IGC network in the transverse direction as can be seen in the side view from Figure 7.8. Prolonged exposure of the samples in the aggressive solution will broaden the IGC attacks which will result in grain interior dissolution and/or fall out. The nature and morphology of intergranular attacks in this current study with and without application of stress are very similar to that found by Fox [235] in unstressed sample under similar experimental conditions. These similarities emphasized the fact that stress is actually increasing the intergranular corrosion kinetics rather than promoting cracking as such.

[34] Details of the 3D volume generation from tomographic slices and the software used for this process are described in Chapter 3.

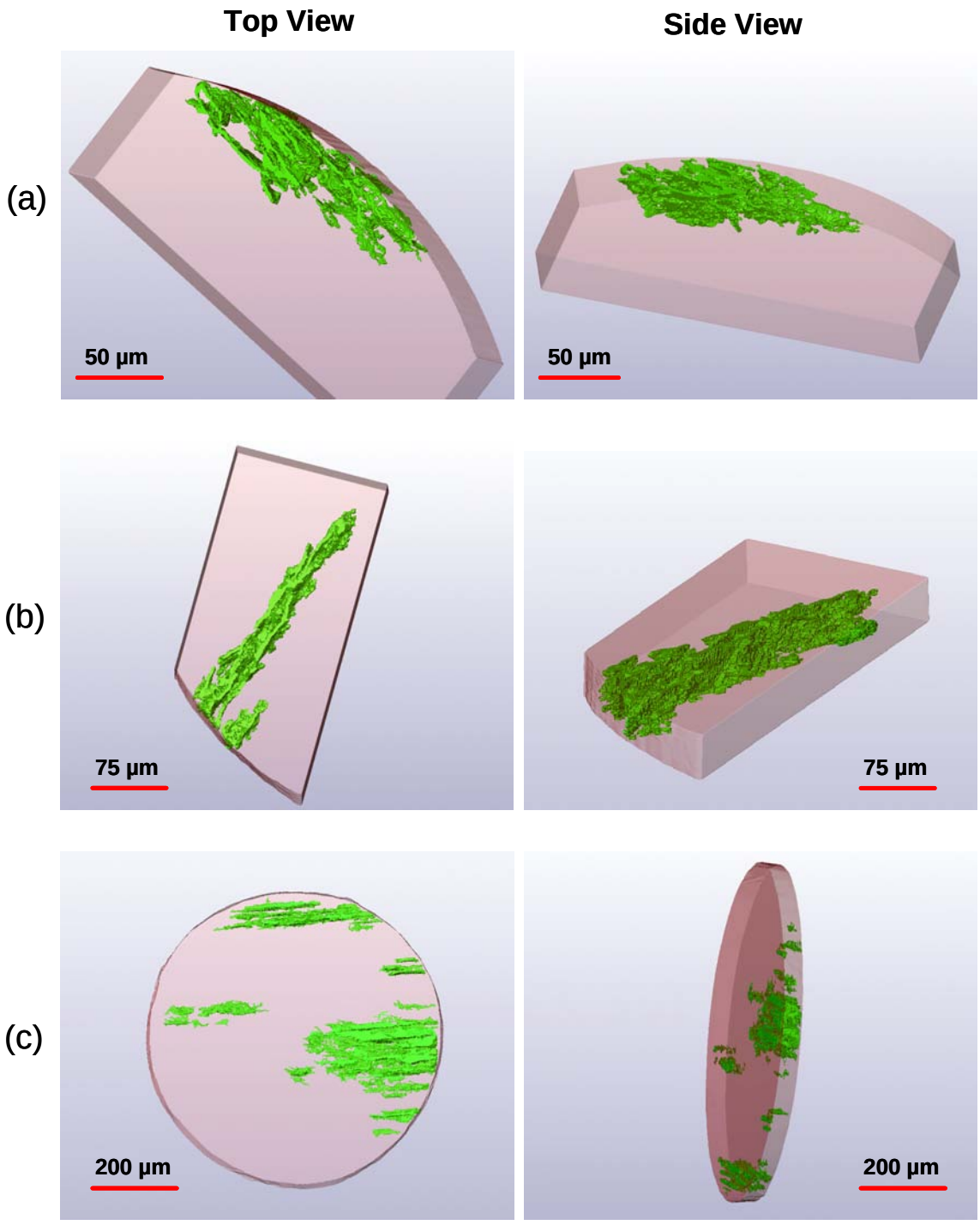

Figure 7.8 Three dimensional reconstruction of some attacked areas (about 150 tomographic slices in each case) in sensitized AA2024 specimens showing top and side view of the intergranular nature of the attacks during their exposure in 0.6M NaCl. (a) Sample with no-stress after 15 h of exposure, (b) 70% YS sample after 16.9 h of exposure, and (c) Sample with 90% YS after 10.9 h of exposure. IGC in 150 slices has been labelled in green.

Figure 7.9 shows the SEM images of the unstressed sensitized temper (i.e., heat treated at 250˚C for 2h) AA2024 specimen after open circuit exposure in 0.6 M NaCl for 35h.[35] The intergranular nature of the corrosion can clearly be seen from these SEM images along with significant grain dissolution and/or grain fall out. Figure 7.9a shows a large attacked area due to extensive grain dissolution/fall out on the cylindrical sample surface. Closer examination on some of the attacked area reveals the presence of more distinct intergranular corrosion (Figure 7.9b-f). Figure 7.9c shows the grain facets in a corroding area after some grains have fallen out due to corrosion. The lateral spread of the intergranular corrosion is speculated to be higher than the depth of the intergranular corrosion attack. These observations are consistent with the fact that corrosion penetration might cease or be limited along the 'L' direction after sometime and different corrosion sites initiated along the 'T' direction on the sample surface coalesce.

Figure 7.10, Figure 7.11, and Figure 7.12 show the 3D reconstruction of the unstressed, 70% Y.S. and 90% Y.S. specimens respectively as a function of exposure time in 0.6 M NaCl. The specimen matrix material has been rendered translucent in order to observe the growth of localized corrosion sites which are labelled in pink colour within the interior of the specimen. Top and side views of the reconstructed samples have been shown to provide a better idea about the evolution of corrosion morphology as well as the location of corrosion attacks.

[35] SEM analysis was performed on the unstressed sample after its last exposure in synchrotron. Sample was taken out from the environmental cell after the completion of synchrotron experiment and cleaned in ethanol. Due to some time lag between the completions of synchrotron experiments and SEM analysis, the sample under SEM may show slightly more corrosion attacks than found from the last scan in synchrotron. However, due to significant amount of corrosion, stressed specimens had lost their mechanical integrity and disintegrated while removing from the stress-rig. So, SEM analysis could not be performed on the stressed samples.

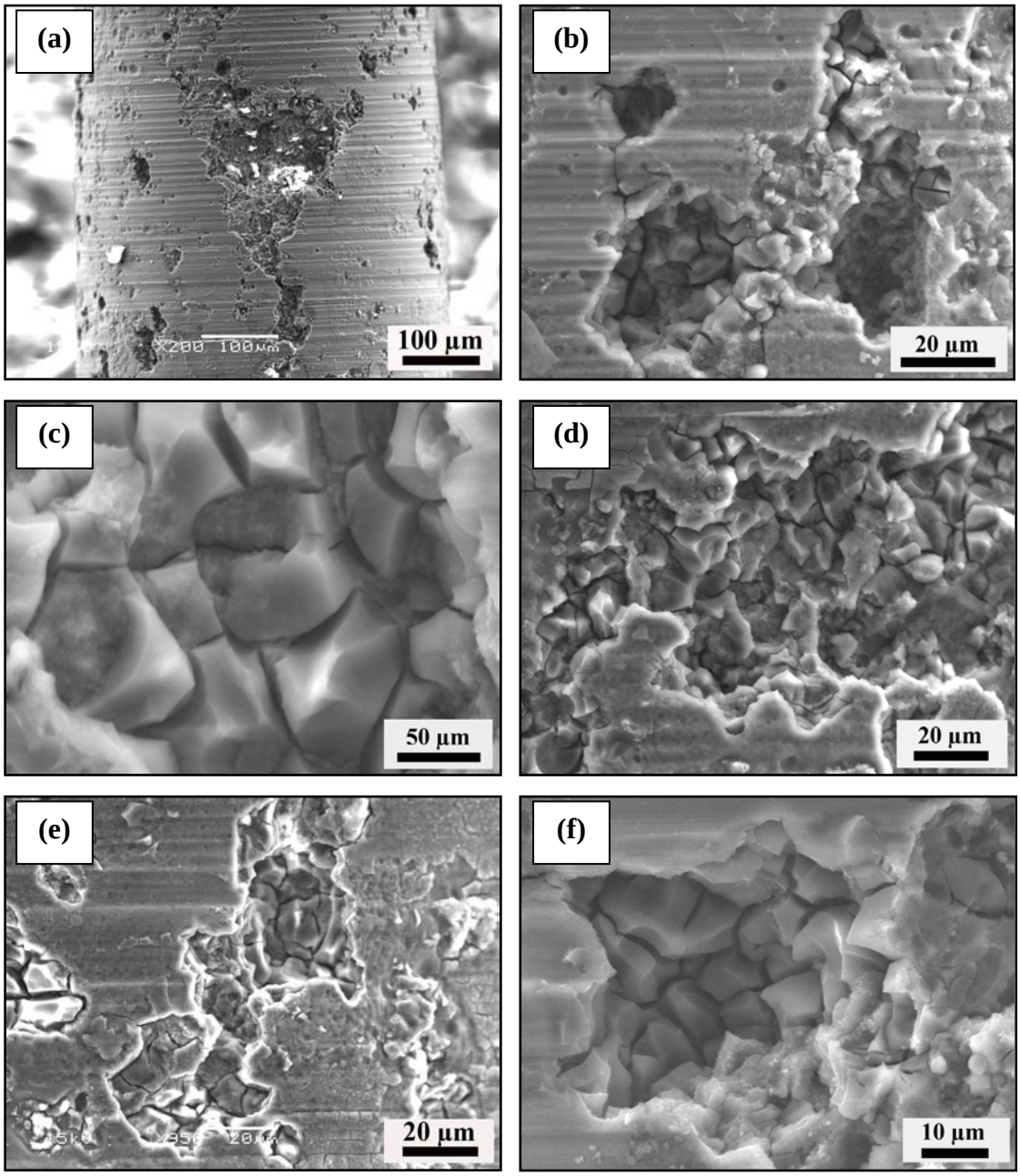

Figure 7.9 SEM images of the unstressed and sensitized (i.e., heat treated at 250˚C for 2h) AA2024 specimen after in situ open circuit exposure in 0.6 M NaCl for 35 h. SEM images are taken after the synchrotron tests. Intergranular nature of the corrosion attacks can clearly be seen from the micrographs. Extensive intergranular corrosion leads to grains fall out from the sample surface and turn into deep pits or holes on the surface at the later stage of exposure. Crystallographic facets of different grains can also be seen at the base of most of the attacks, (c) and (f).

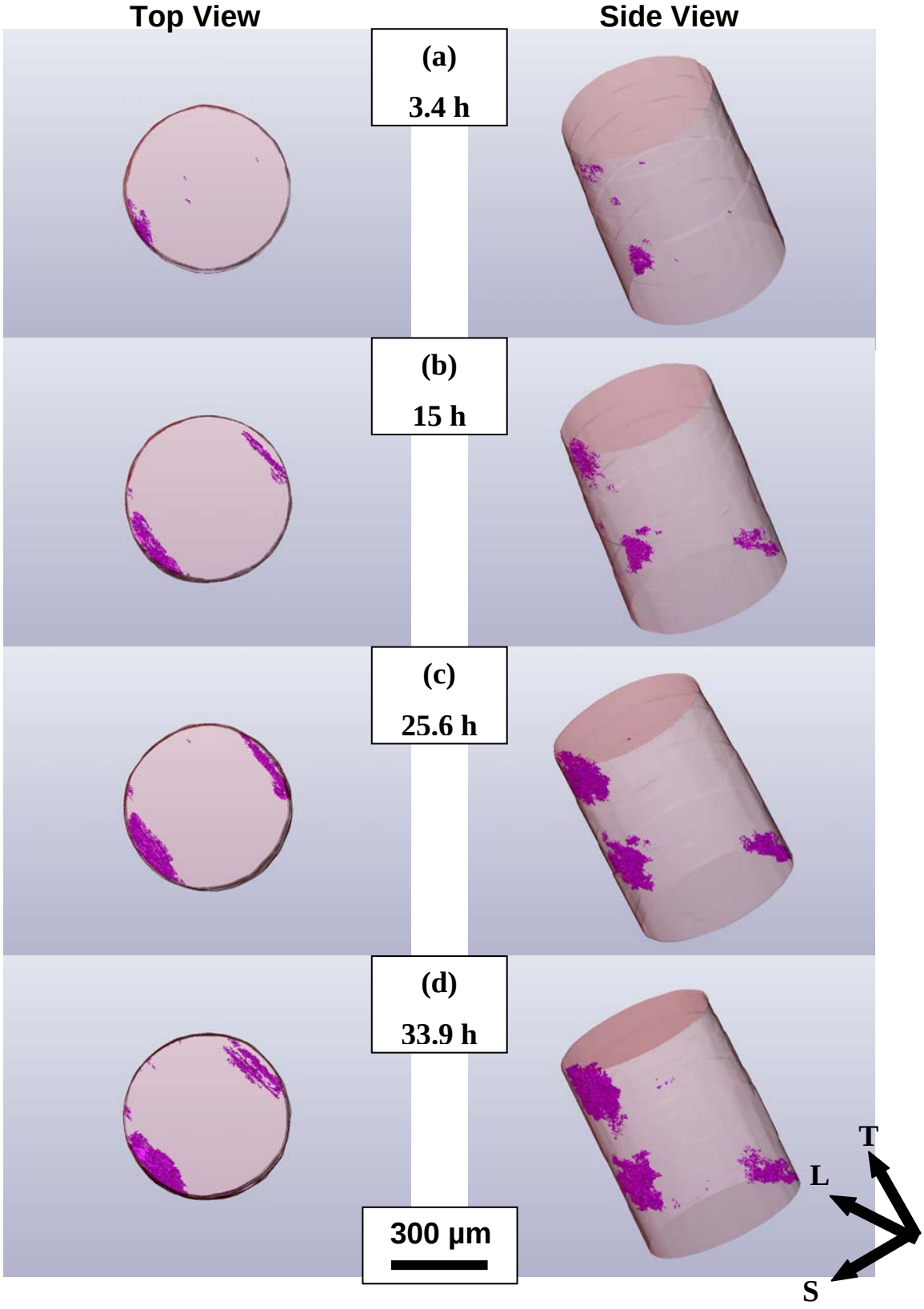

Figure 7.10 Top and side views of the three dimensional reconstructed images (about 1000 tomographic slices in each case) showing the evolution of IGC in the sensitized AA2024 specimen (i.e., heat treated at 250˚C for 2h) in unstressed condition after in situ open circuit exposure in 0.6 M NaCl as a function of time, i.e., (a) 3.4 h, (b) 15 h, (c) 25.6 h, and (d) 33.9 h of exposure. Intergranular corrosion has been labelled in pink colour.

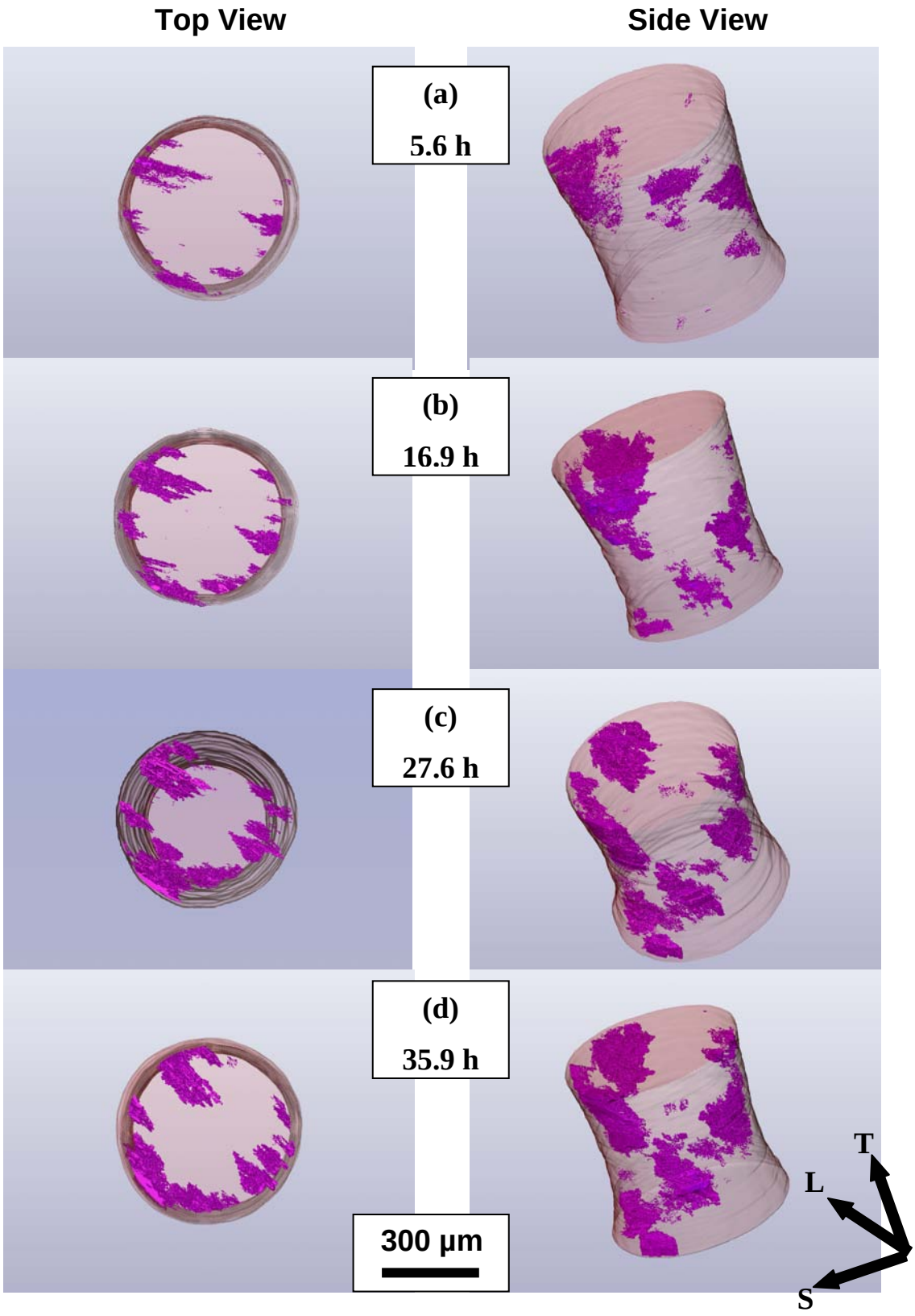

Figure 7.11 Top and side views of the three dimensional reconstructed images (about 1000 tomographic slices in each case) showing the evolution of IGC (labelled in pink colour) in the sensitized and stressed (70% yield strength) AA2024 specimen after in situ open circuit exposure in 0.6 M NaCl as a function of time, i.e., (a) 5.6 h, (b) 16.9 h, (c) 27.6 h, and (d) 35.9 h of exposure. Stress is applied in transverse direction, T.

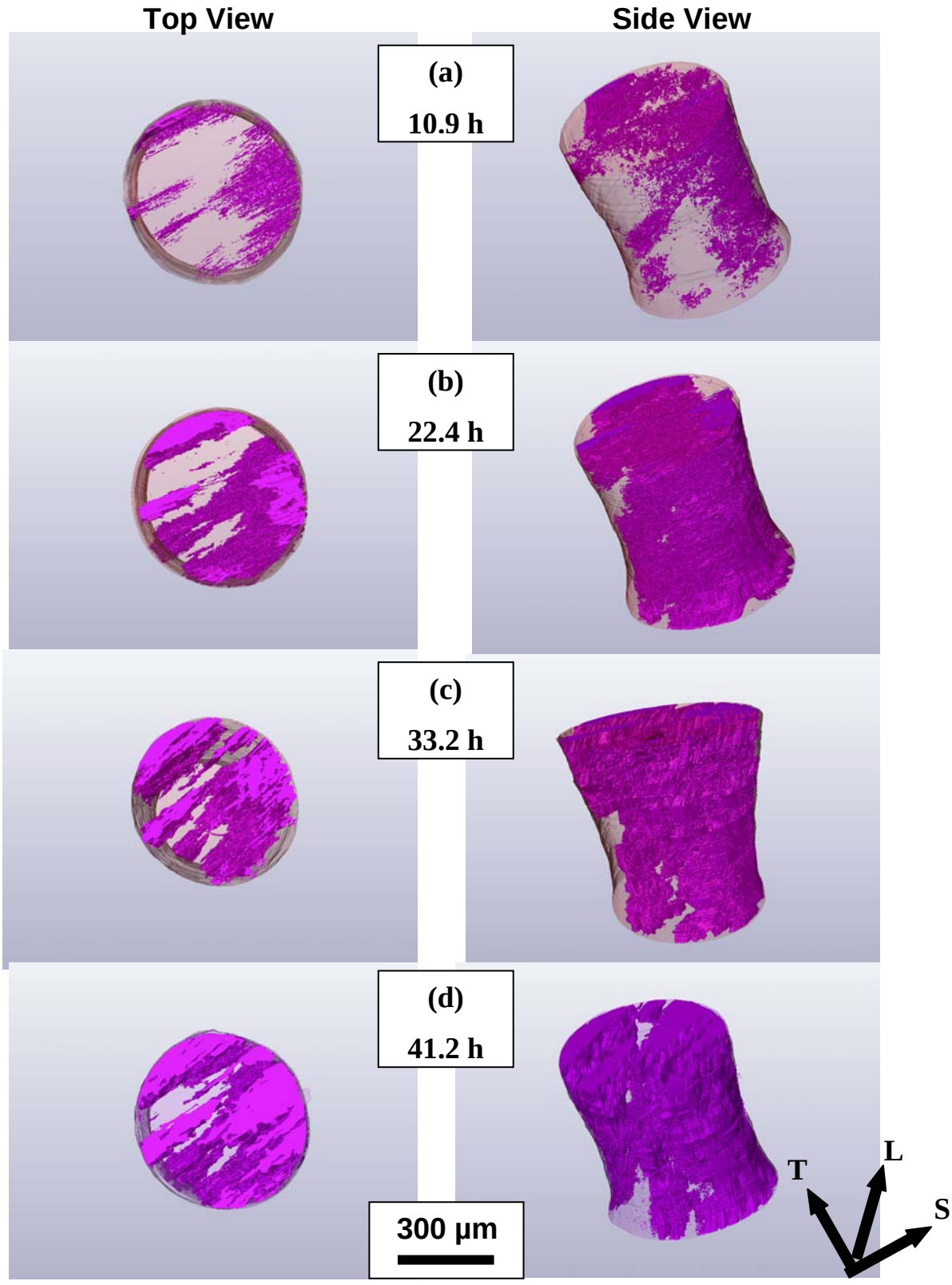

Figure 7.12 Top and side views of the three dimensional reconstructed images (about 1000 tomographic slices in each case) showing the evolution of IGC (labelled in pink colour) in the sensitized and stressed (90% yield strength) AA2024 specimen after in situ open circuit exposure in 0.6 M NaCl as a function of time, i.e., (a) 10.9 h, (b) 22.4 h, (c) 33.2 h, and (d) 41.2 h of exposure. Stress is applied in transverse direction, T.

Figure 7.10 shows that in an unstressed AA2024 specimen, localized corrosion initiates at few particular sites on the sample surface while most of the surface remains unattacked. Figure 7.11 shows the evolution of localized corrosion in the dog-bone AA2024 specimen stressed to 70% Y.S. Intergranular corrosion attacks initiates at the surface and propagates in the 'L' direction. However, IGC growth in L direction ceases or is limited after a certain time, but corrosion initiates at other places of the sample surface. AA2024 specimen with 90% YS (Figure 7.12) show much more corrosion attack compared to the unstressed or 70% stressed samples. Significant amounts of metal loss due to the grain dissolution and/or grain fall out can be seen even after 11 h of exposure. In most of the cases growth of the localized corrosion sites into the bulk of the specimen seems to be followed by the general dissolution of the grain interiors and/or grain fallout, resulting in considerable metal loss.

The effect of applied stress on the evolution of localized corrosion can easily be seen from these figures (Figure 7.10, Figure 7.11, and Figure 7.12). Comparisons of these three figures clearly establish that intergranular corrosion is much more severe under the application of stress. The sample stressed to 90% YS has shown a considerable amount of intergranular corrosion. It can be seen from the tomographs that the attack follows the rolling direction of the alloy. The rate of growth in through thickness or short transverse (S) direction is much slower than in the longitudinal (L) or long transverse directions (T) directions.

The ability of X-ray synchrotron tomography technique to visualize the localized corrosion within the bulk of opaque specimen can clearly be established from Figure 7.13, Figure 7.14, and Figure 7.15. These 3D reconstructions of the specimens are produced by combining the information contained in a full tomographic scan data volume, consisting of 1024 slices.

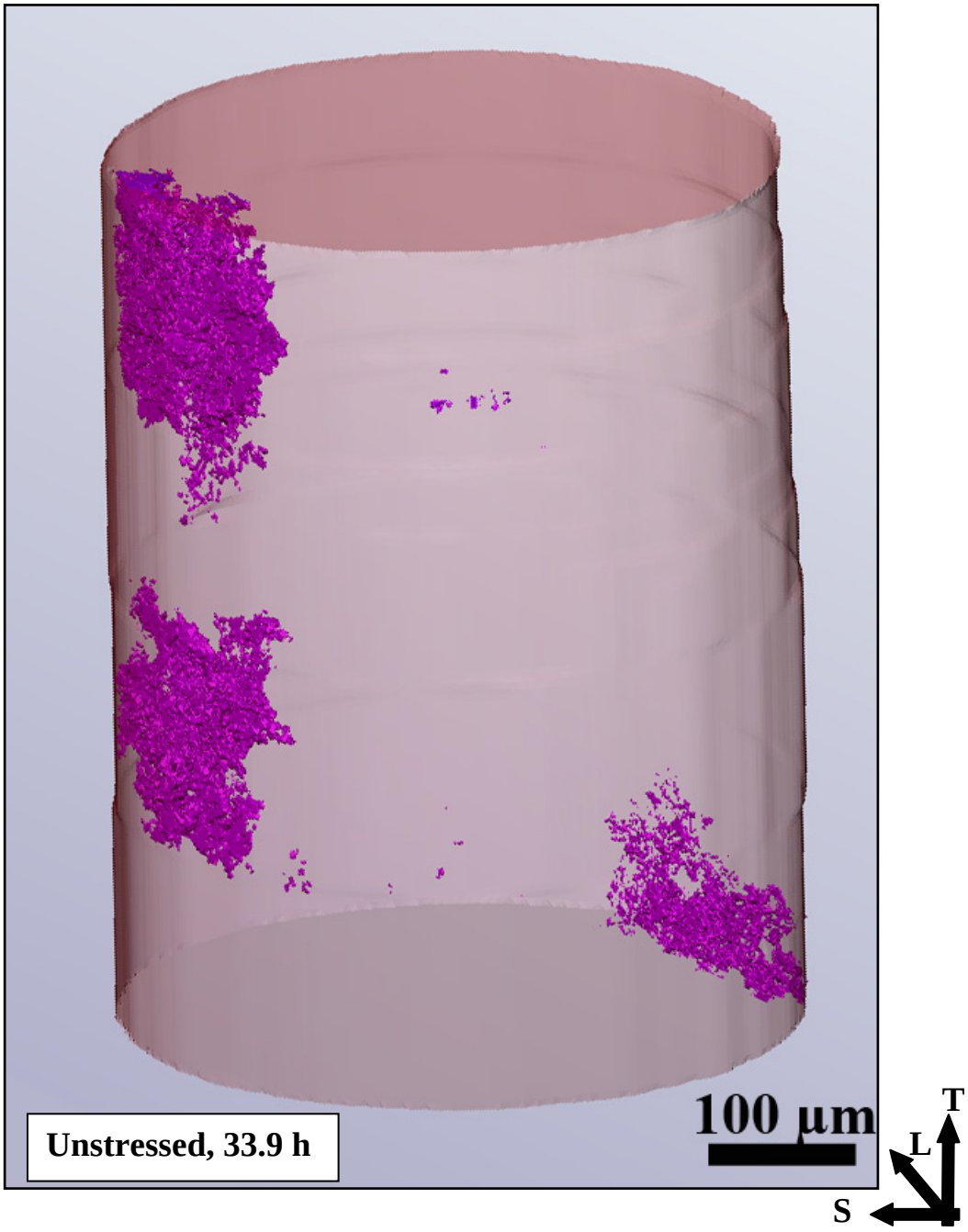

Figure 7.13 Three dimensional reconstructed image (about 1000 tomographic slices in each case) showing the morphology of IGC attacks in the sensitized AA2024 specimen (i.e., heat treated at 250˚C for 2h) in unstressed condition after in situ open circuit exposure in 0.6 M NaCl for 33.9 h. Intergranular corrosion has been labelled in pink colour.

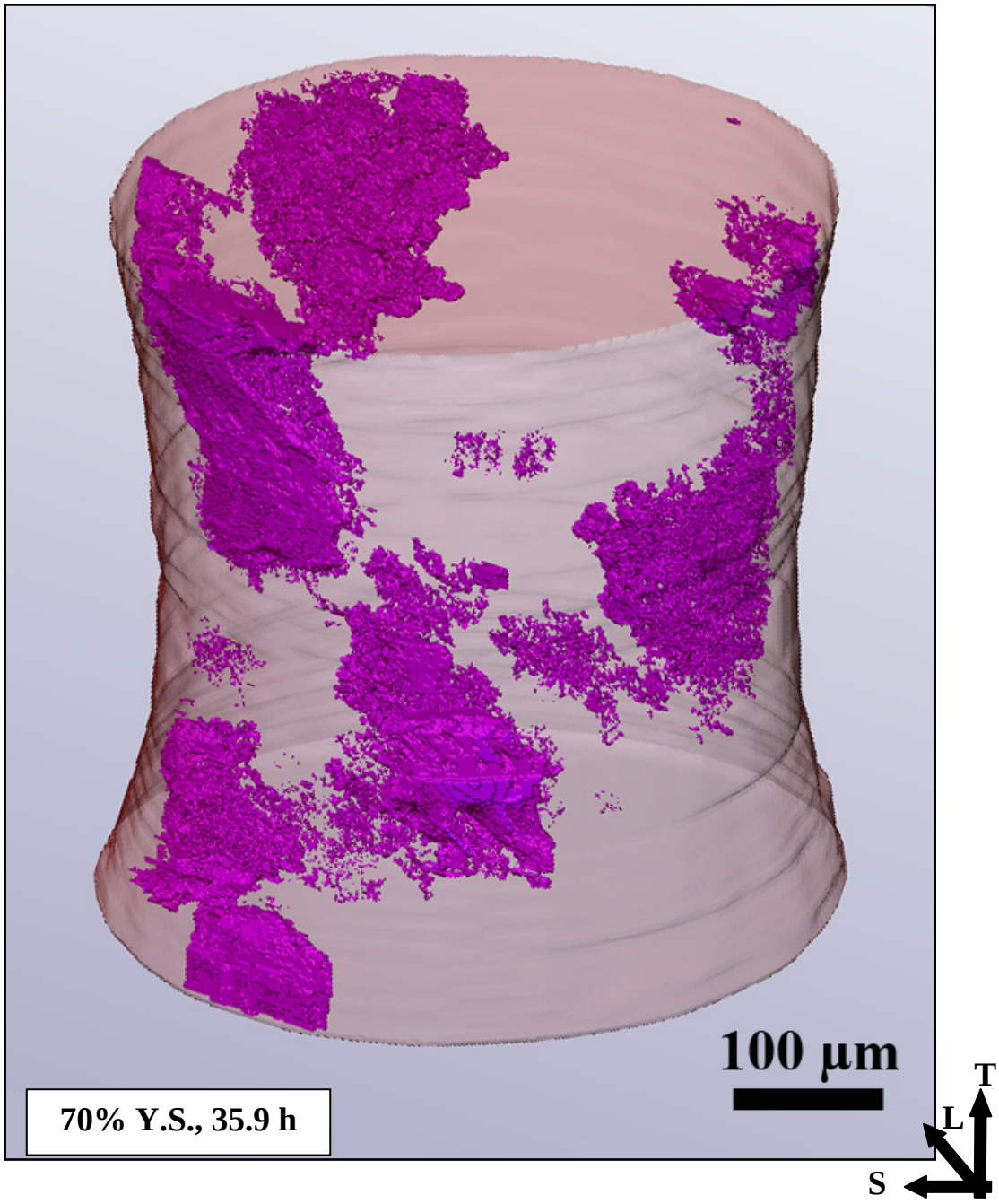

Figure 7.14 Three dimensional reconstructed image (about 1000 tomographic slices in each case) showing the morphology of IGC attacks in the sensitized (i.e., heat treated at 250˚C for 2h) and stressed (70% Y.S.) AA2024 specimen after in situ open circuit exposure in 0.6 M NaCl for 35.9 h. Intergranular corrosion has been labelled in pink colour.

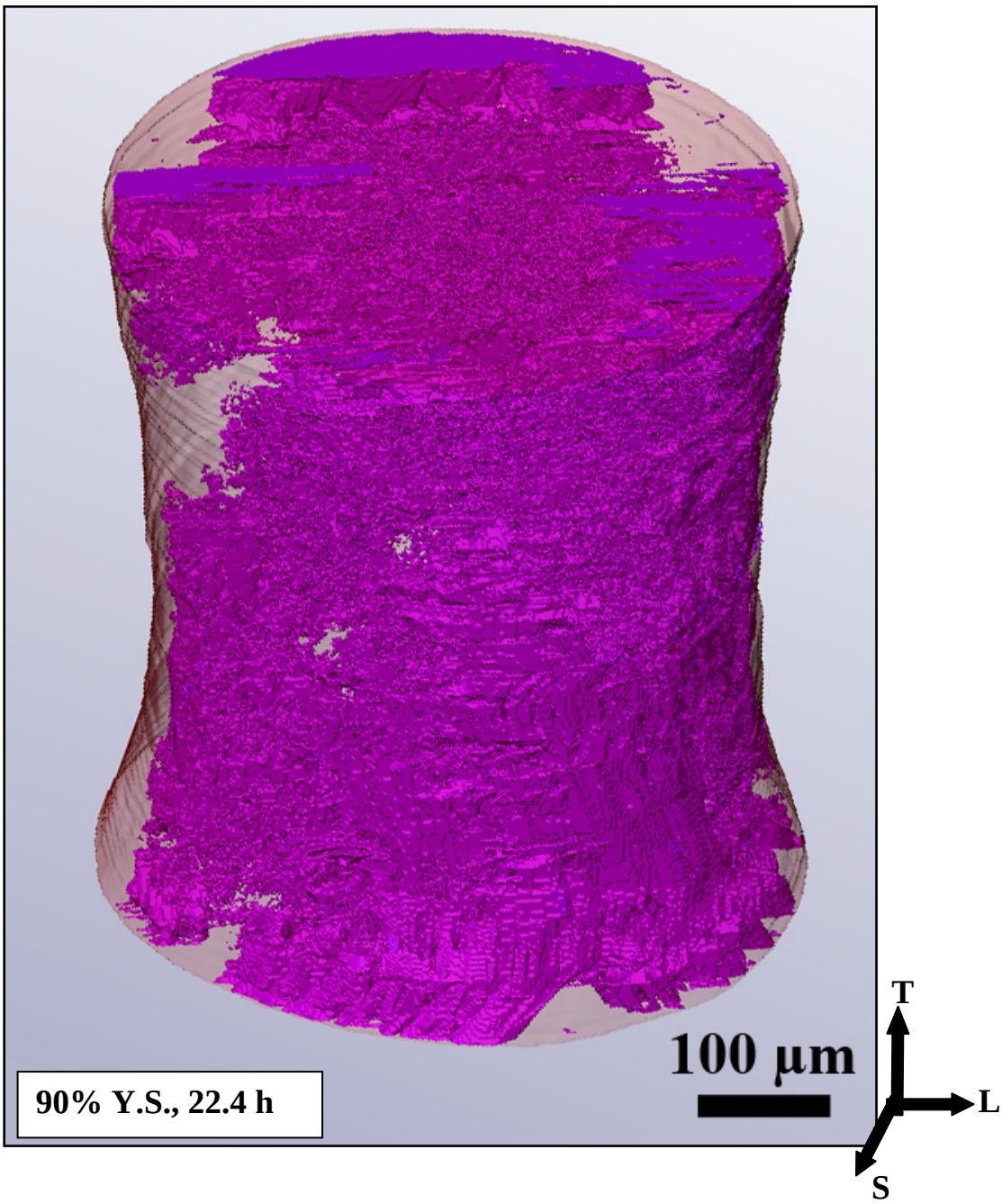

Figure 7.15 Three dimensional reconstructed image (about 1000 tomographic slices in each case) showing the morphology of IGC attacks in the sensitized (i.e., heat treated at 250˚C for 2h) and stressed (90% Y.S.) AA2024 specimen after in situ open circuit exposure in 0.6 M NaCl for 22.4 h. Intergranular corrosion has been labelled in pink colour.

Figure 7.13, Figure 7.14, and Figure 7.15 are basically similar to the 3D reconstructions already shown in Figure 7.10, Figure 7.11, and Figure 7.12. However, in these cases the 3D views of the specimens are enlarged to establish the usefulness of X-ray synchrotron tomographs to pick up very small details of the features present within an object. The number, size, and morphology of all the localized corrosion sites within the specimen can clearly be quantified from these three dimensional figures. It has to be noted that though these pictures present the specimen view from a particular orientation, the 3D specimen object can be rotated freely using the software to a particular orientation of interest. In all cases the specimen interior has been made translucent to have a clear view of the localized corrosion sites which are labelled in pink colour.

Figure 7.13 shows the 3D reconstruction of the unstressed specimen after 34 h exposure in 0.6 M NaCl. Three predominant IGC corrosion sites can be seen in the matchstick cylindrical specimen. Spread of these IGC sites are more in the L and T direction than in the S direction. The specimen stressed to 70% YS (Figure 7.14) shows similar corrosion features to that observed on the unstressed sample except that the stressed specimen is more severely attacked. Several intergranular corrosion sites can be seen after 36 h of exposure. Figure 7.15 shows extensive localized corrosion in the 90% YS specimen interior after 22 h of exposure. Rapid IGC growth seems to be followed by grain dissolution resulting in the significant material loss.

7.3 Quantitative IGC Growth Rates in Unstressed and Stressed Specimens as a Function of Immersion Time

Instead of using a linear measurement of IGC growth in a single direction, this current study quantifies the IGC damage by measuring the volume of material loss due to the overall IGC event which includes the widening aspect of the localized corrosion.[36]

The amount of IGC attack (represented as volume of metal loss as a percentage of specimen volume)[37] on the unstressed and stressed specimens as a function of exposure time in naturally aerated 0.6 M NaCl solution is shown in Figure 7.16. In the same figure, IGC growth in sample without stress and sample with 70% YS has been emphasized in a separate graph. It is quite obvious that stress is contributing significantly in the increase of intergranular corrosion growth kinetics as expressed by the volume loss with increasing exposure time. However, a huge difference in the IGC volume loss has been noticed between the samples stressed to 90% of its yield strength and the sample stressed to 70% of its yield strength. Intergranular corrosion of aluminium alloys are associated with an induction period prior to the initiation [70, 95]. So, it could be possible that the induction period is followed by initiation of IGC and rapid propagation. Due to the limited number of exposure of each specimen under the synchrotron (4 times during the span of almost two days), it was difficult to get more information about the initiation stage.

[36] More details about the quantitative IGC growth rate measurement in a single direction as well as IGC damage represented by the volume of material loss can be found elsewhere [235].

[37] Depending on the geometry of the specimen (‘matchstick’ vs. ‘dog-bone’ types), exposed area under the synchrotron may vary. So, total volume losses due to IGC from a specimen as well as the total volume of that particular exposed specimen were calculated using the software ‘Amira’. Ratio of these two (i.e. total volume of IGC loss : volume of the exposed specimen) are represented in the graph.

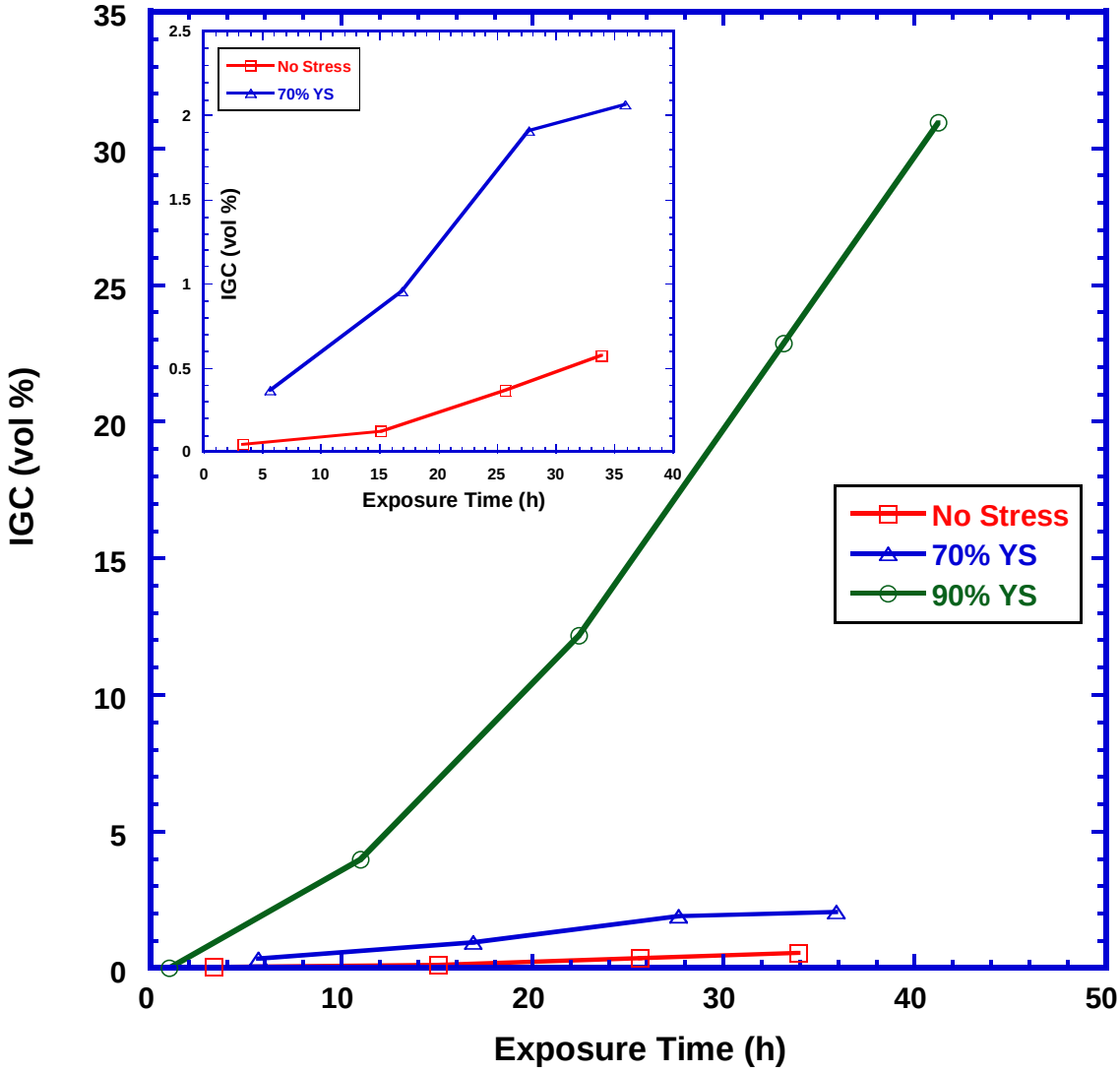

Figure 7.16 IGC in the form of volume of metal loss as a percentage of sample volume in the sensitized (i.e., heat treated at 250˚C for 2h) AA2024 specimen in unstressed and stressed condition after in situ open circuit exposure in 0.6 M NaCl as a function of time. It can be seen that volume loss is significantly high in the sample stressed to 90% of yield strength. Samples stressed to 70% YS also show higher volume loss than the unstressed sample. Comparison of unstressed and 70% YS sample is shown separately in the inset graph.

However, IGC growth at the later stage of exposure of for all samples is presented in Figure 7.17. It can be seen clearly that in the later stage of IGC growth both unstressed and 70% YS samples followed similar linear growth rate relationships, whereas 90% YS

sample is markedly different with much higher slope in the linear growth rate. After 40 hours of exposure, the 90% YS sample lost almost 30% of its volume due to intergranular attack.

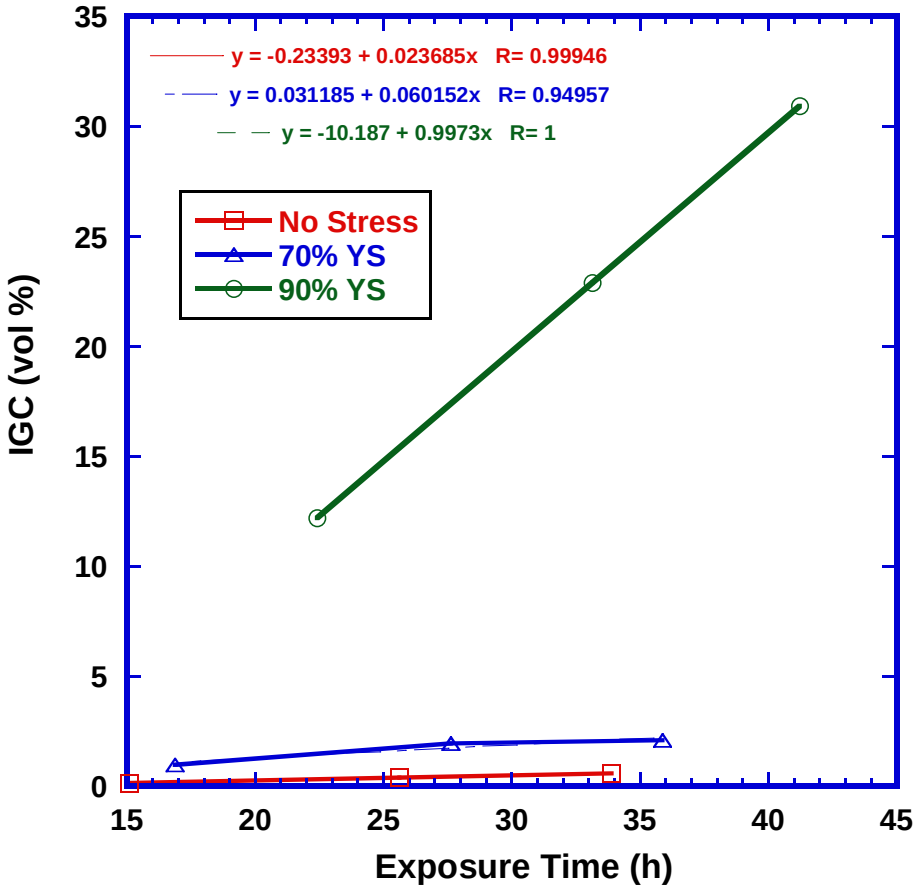

Figure 7.17 IGC in the form of volume of metal loss as a percentage of sample volume at the later stage of exposure of the sensitized (i.e., heat treated at 250˚C for 2h) AA2024 specimen in unstressed and stressed condition during in situ open circuit exposure in 0.6 M NaCl. It can be seen from the best fit of the curves that IGC growth follows a linear relationship with time. The slope for the 90% sample is much higher than the unstressed and 70% YS sample indicating higher amount of material loss due to IGC with higher stress.

7.4 Discussion

The advantages of the X-ray synchrotron technique over the conventional 2D techniques have been discussed in Section 2.4 of Chapter 2 and in the beginning of this chapter. The results from this current study not only demonstrate different features/information that can be obtained from the bulk material, but it also shows the enormous potential of the X-ray synchrotron tomography as a very useful non-destructive technique. This study also establishes the effect of applied stress on localized corrosion (predominantly intergranular corrosion) propagation in aluminium alloys. Standard electrochemical tests and subsequent microstructural analysis of the exposed samples can provide information about the susceptibility of a material towards localized corrosion. However, as most of these conventional techniques are based on observations in two dimensions, they can not provide information about the true shape, connectivity, morphology and sizes of the localized corrosion sites. Information about the development of such localized corrosion sites as a function of exposure time or its interaction with microstructural features can not be obtained either. Hence, difficulties remain with the conventional 2D techniques to accurately measure localized corrosion growth rates.

This current study demonstrates that X-ray synchrotron tomography can be used to visualize and characterize the development and quantify the growth rates of localized corrosion sites. High voxel[38] resolution (~ 0.7 μm) in the current study allows the possibility of very detailed and accurate study of the interior of the specimen in both two and three dimensions. Analysis software also allows the flexibility to view a particular specimen in three dimensions (or a single slice of a specimen at a particular plane in two

[38] A voxel is a three dimensional pixel.

dimensions) at any position and any orientation. These flexibilities associated with this technique help in monitoring and quantifying the localized corrosion growth in S, L or T directions. However, it should be noted that human error during the use of the software (Amira) can result into the inaccurate quantitative analysis. During 3D data analysis using the software, voxels of different features are labelled from their respective contrast values. As the threshold values used to differentiate these regions are set by the person performing the analysis, any human misjudgement could lead to the inaccuracy of the analysis [235].

Apart from these, the limitations of the specimen size and spatial resolution during the synchrotron experiments could potentially result into the underestimation of growth rates. As the X-ray tomographic technique depends on the transmission of the beam through the specimen, energy used during the experiment often limits the size of the specimen to be used. With beam energy of 17.5 keV, 500 μm diameter specimens are used in this current study to ensure sufficient transmission of the incident X-ray beam. Small sample size may affect the penetration kinetics in a particular direction. For examples, in many cases during the current study IGC is seen to be rapidly penetrated the thickness of the specimen in the L direction. So, it is quite possible that with larger diameter of the specimen further growth would have been observed. It is also speculated that small sample size can limit the amount of anodic dissolution by providing smaller surface area for supporting cathodic reaction [235].

As described earlier (Chapter 2), aluminium alloy 2024 is characterized by the presence of intermetallic particles which have high atomic numbers compared to the matrix and as a result they appear white in the tomographs with significant contrasts. It is believed that these intermetallic particles are associated with the initiation sites of

localized corrosion in the alloy [8].[39] So, detailed investigations have been performed earlier at the University of Birmingham to obtain a better understanding on how the presence of intermetallic particles affects the propagation of intergranular attack [235, 288]. Connolly *et al.* [288] described the appearance of different features in a tomographic slice of sensitized AA2024 in great detail. The main features of a particular tomographic slice (Figure 7.1) of this current study is consistent to that reported by Connolly *et al.* [288]. It is quite clear from these tomographic images that X-ray tomography can be used accurately to image and measure different features like intermetallic particles which are aligned in the rolling direction, pre-existing cavities in the matrix and adjacent to the particles, localized attack and their interactions with the microstructural features etc.

3D reconstructions of some corroded areas from both unstressed and stressed specimens (Figure 7.8) along with the after-exposure SEM analysis of the unstressed specimen (Figure 7.9) suggests the intergranular nature of the localized attack during this current study. All attacks in this current study (in both stressed and unstressed sensitized temper specimens) are found to be intergranular in nature with absence of any cracking even after 36h of exposure in this particular environment (0.6 M NaCl). Intergranular corrosion is a type of localized attack at and adjacent to the grain boundaries as a result of an enhanced thermodynamic and/or kinetic tendency for corrosion relative to the grain matrix [111, 217]. IGC is operated by a pre-existing active dissolution path based on compositional/structural heterogeneity. In AA2024 intergranular corrosion is believed to start with the dissolution of the S phase particles (Al_2CuMg) on the grain boundaries

[39] Detailed discussion about the role of intermetallic particles in the initiation of localized corrosion can be found in the literature review (Chapter 2) and in Chapter 5 (Microelectrochemical studies on single intermetallic particles).

caused by the galvanic coupling between the solute-depleted zone/surrounding matrix and solute-depleted zone/S phase particles [7]. Subsequently, IGC propagates by the dissolution of the copper depleted zone along the grain boundaries [95].[40]

Anisotropic growth of localized corrosion in AA2024-T3 has been confirmed by several researchers and it was also found that the 2D penetration rate of localized attack depends on the direction of the applied stress [29, 52, 233, 319]. So, it is important to know the orientation of the sample under examination to have a proper idea about the localized corrosion growth in three dimensions. Figure 7.2 shows the schematic of a typical specimen with these three different orientations. Stressed samples were subjected to load in the transverse (T) direction. Figure 7.2 also schematically explains how a single slice from a single plane is represented within the bulk specimen.

In both unstressed and stressed specimens, IGC attacks are found to be propagated in the L direction at a faster rate (Figure 7.4- Figure 7.6). As the L direction in the specimen is also the rolling direction of the source plate, it is possible that IGC attacks are following the easier paths of longer grains. Spread of the IGC attacks in the S direction is smaller than in the L and T direction. These observations are consistent with the other researchers [233] who reported slow growth rate of IGC in S direction as a result of longer path resulting from 'squeezed' grains in the short transverse direction. It is also evident from the 2D tomographs that localized corrosion does not necessarily initiate from the intermetallic particles every time and is therefore consistent with the findings of others [235]. However, the amount of localized corrosion attack in the presence of stress is much higher than in the unstressed condition. In some cases, severe undercutting of the stressed specimen surfaces have been seen (Figure 7.6b and c). This may be an indication

[40] Mechanisms of intergranular corrosion in aluminium alloys and its relation with different heat treatment could be found in Section 2.2.2 of Chapter 2.

that the machining process for manufacturing the specimens can actually affect the corrosion susceptibility and the rate of local attacks on the surface [288].

As seen in unstressed samples, IGC in stressed samples also stops growing (or the growth rate significantly decreases) in the L direction and broadening of IGC occurs through grain interior dissolution and/or grain fall out. Volume analysis in three dimensions (3D) [Figure 7.10, Figure 7.11, and Figure 7.12] showed an increase in volume loss as a function of time which proves that, though IGC stop growing in L direction, it continues to grow in other directions. It is very possible that for both stressed and unstressed samples many localized corrosion sites might initiate as pitting attacks which later develop as intergranular corrosion.

As discussed earlier, the localized corrosion attacks in the current study seems to follow the elongated grains in the rolling direction (see Figure 7.8). Prolonged exposure in an aggressive solution will lead to the coalescence of these attacks and forming of a plate like IGC network in the transverse direction as can be seen in the side view from Figure 7.8 (more elaborative view of the IGC network within a specimen interior can be seen in Figure 7.13, Figure 7.14, and Figure 7.15). The nature and morphology of intergranular attacks in this current study with and without application of stress are very similar to that reported by Fox [235] in unstressed sample under similar experimental conditions. These similarities emphasize the fact that stress is actually increasing the intergranular corrosion kinetics rather than promoting cracking as such.

The influence of mechanical/applied stress on the kinetics of intergranular corrosion is complex and has been debated. Stress corrosion cracking is driven by the synergistic actions of mechanical and electrochemical factors. So, it is thought that IGC and IGSCC are closely linked phenomena, and it has been viewed by some researchers that IGSCC is nothing but stress assisted IGC [29]. However reported experimental

results are contradictory and can be divided into main groups like: (a) stress induced intergranular corrosion, and (b) stress assisted intergranular corrosion [218]. When in a mechanically stressed specimen, intergranular attacks occur under less aggressive electrochemical conditions compared to the unstressed condition, it is known as stressed induced intergranular corrosion. By comparison, if under identical electrochemical conditions, the growth rate of intergranular attacks is higher in mechanically stressed specimens, it is known as stress assisted intergranular corrosion. According to this convention, as both unstressed and stressed specimens in the present study are in identical electrochemical condition and application of stress seems to increase the kinetics of intergranular corrosion, the observed attacks in the stressed sample in this current study can be classified as stress assisted intergranular corrosion.

As the accurate IGC rates are difficult to quantify using conventional two dimensional measuring methods, the X-Ray tomography is probably one of the most valuable tools to quantify IGC growth rate in 3D. Earlier studies by the foil penetration technique [29, 233, 320] showed that growth rate of localized attack was anisotropic because the attack was intergranular corrosion (IGC) and the grains were elongated in the rolling direction. In the foil penetration technique, the growth kinetics of localized corrosion is measured by the time required to penetrate a thin foil [29, 49-52]. Liu *et al.* [29, 319] studied the effect of tensile stress on the intergranular corrosion of AA2024-T3 using a modified foil penetration technique. This group also used X-ray radiography[41] to image in situ initiation and growth of multiple IGC sites in AA2024 in unstressed

[41] X-ray radiography captures the 2D radiographic projection of the samples whereas in X-ray tomography a series of recorded 2D radiographic projections (taken while the sample is being rotated from 0˚ to 180˚) are used to reconstruct a 3D map of the X-ray attenuation coefficient of the material using appropriate algorithm.

condition as well as under the application of normal tensile stress [53-55]. It was found that the penetration rate of corrosion attack depends on the applied potential and stress state with samples showing higher penetration rate when subjected to an applied load.

However, the main disadvantage with the foil penetration technique is that it determines the growth kinetics of the fastest growing localized corrosion sites. In this present study it has been observed several times that IGC growth might cease or be limited in a particular direction (e.g., in many cases IGC attacks stops growing in the L direction), but continues in other directions. These observations emphasize the limitations of foil penetration technique. Increase in the IGC rates in the presence of a tensile stress at the surface of the material was also reported by Rota et al. [218]. Zhao *et al.* [55] studied the intergranular corrosion of aluminium alloys using X-Ray radiograph and found that growth kinetics determined from radiographs of the samples were slower than growth kinetics determined by foil penetration technique. In a separate study Zhao and Frankel [35] investigated the effect of prior deformation on localized corrosion of aluminium alloys. AA2024-T3 showed increased corrosion rate after pre-stressing, but little change in breakdown potentials. It is speculated that the increase in the current density with increase in pre-strain is due to the deformation induced defects.

It was also found that the nominal growth rate in the short transverse (S) direction is slower because of the longer path length around the grains in that direction.[42] It is confirmed from this study that corrosion propagates at a much faster rate in the L and T direction in both stressed and unstressed specimen. The distribution of IGC in the T direction (which is also the stressing direction) can be seen from the three dimensional

[42] Refer back to Figure 2.23 (Chapter 2) for grain structure in different directions of AA2024.

rendering of the samples, Figure 7.10 - Figure 7.12. IGC attacks seem to be initiated from the edge of the surface and propagate in the L direction until a certain depth.

Rapid growth of IGC to a certain depth and its subsequent cease or limit in growth rate could possibly be explained by the self-limiting effect of localized corrosion as discussed by Lifka [221]. IGC initiate and grow rapidly to a certain depth at which it becomes mass transport limited. Growth of the IGC attacks then decrease significantly since it becomes more difficult for the oxygen and the corroding species to transport down to the active tip of the IGC site through the narrow and tortuous corrosion path. Severe branching of IGC networks make it extremely difficult for oxygen to diffuse down to the active tip to provide necessary cathodic support for continuing anodic dissolution. Application of stress is thought to play an important role at this stage. Stress would tend to rupture any film that might form at the IGC tip and also effectively open up the IGC path, thereby increasing mass transport and decrease the ohmic potential drop down the narrow IGC path [29, 218]. When penetration of IGC in a certain direction ceases, it begins to spread laterally through the material in other directions [221].

This theory has been experimentally supported by the three dimensional visualization of IGC by Fox [235], who found that IGC sites rapidly penetrate a susceptible alloy to the limiting depth at which point the electrochemical driving force for corrosion would start favouring the grain interiors rather than the grain boundaries. At this point widening of IGC will occur as found in this current study and also observed by other researchers [52, 321]. Augustin *et al.* [321] studied the kinetics of intergranular corrosion in AA2024-T351 by immersing the samples in 1 and 3 M NaCl followed by optical and SEM observations on the sectioned samples. Augustin found that the intergranular corrosion corresponds not only to an increase in the depth of the corrosion attacks but also an increase of the width of the attacks. During their study, depth of

penetration of IGC attacks in AA2024-T351 remained the same between the exposure time of 72 and 168 hours; however, the IGC attacks of the 168 h immersed samples were much wider compared to the 72 h exposed samples. The dissolution of the interior grains could also result due to the possible change in chemistry inside a dissolving boundary.

Kotsikos *et al.* [236] suggested that aggressive ion accumulation inside an active tip of an IGC can occur within a few hours. This increase in aggressiveness could play an important role in spreading the dissolution from the boundaries to the grain interiors. Though growth ceases or is limited in the L direction, the localized corrosion sites start widening up in the S direction as well as continuing their growth in the T direction. Several active sites in the T direction from the outer surface of the exposed sample would then coalesce, thereby contributing to the volume loss of the material. Propagation of IGC as a function of time in the S direction is slow and that can be observed from the 3D and 2D figures. Grains fall out from the matrix as the IGC attack becomes significant and surrounds a grain in three dimensions. Wedging stress generated by the corrosion product inside the IGC attack may also play an important role in assisting the IGC process [29, 53]. Local wedging stress from the corrosion product could be significant enough to prevent repassivation in the localized corrosion environment.

Detailed quantification of the growth rate of IGC in aluminium alloys has been limited in the open literature. In most of the studies growth rate has been measured as 2D penetration in different orientations.[43] IGC growth is normally found to follow a t^n penetration relationship which is represented as $d = Kt^n$, where d is the depth of penetration, K is a constant, t is time and n is a fraction between 0 and 1 [29, 55, 319, 320]. However, it should be noted that in most of these cases, the test specimens were

[43] See Section 2.2.2.1 (Chapter 2) for more details about Growth Kinetics of IGC in Aluminium Alloys.

polarized above the pitting potential of the alloy. Hence, it is possible that under those experimental conditions grain boundary dissolution is accelerated and therefore the IGC rates measured are not really representative of what an alloy might encounter in real service life. It is interesting to note that, when in this current study the intergranular corrosion growth rate is measured in three dimensions and represented as volume loss as a function of exposure time, the growth rate seems to follow a linear relationship (see Figure 7.17).

Rota and Boehni [218] speculated that the effect stress on the growth kinetics of localized corrosion is strongly dependent on the number of parallel growing attacks/cracks in the exposed area. Intergranular corrosion growth of AA2024 under applied stress was divided in three subsequent stages: (i) activation, (ii) transition, and (iii) stable, macroscopic grain dissolution stage. Effect of stress was found to be only in the first stage where a small number of parallel cracks/localized attacks were active. In the second stage those localized attacks starts forming network and branching, thereby making the effect of stress less predominant. In the third stage, grain dissolution starts and growth kinetics become independent of applied stress. Rota tried to explain the effect of stress based on stress induced widening of the attacks which not only reduces the integral ohmic resistance of the system but also improves the mass transport rate. With the generation of large number of parallel cracks/localized attacks and network formation, chances of stress induced widening of IGC attacks diminished. This phenomena result into the disappearance of stress effects in the presence of large number of parallel IGC attacks. However it must be noted that Rota's model of stress induced IGC growth kinetics is based on the results obtained from a modified foil penetration test set up which measure the fastest growing localized attack in two dimensions.

Observations of the localized corrosion growth kinetics in two dimensions in this current study are quite similar to that reported by Rota and Boehni [218] in the stressed and unstressed conditions. Initial rapid growths of the intergranular attacks in the L direction have been found for both stressed and unstressed sample (Figure 7.4 - Figure 7.6 and Figure 7.10 - Figure 7.12) before reaching self-limiting growth. However, in all the cases grain dissolution continues as a function of immersion time as seen from the three dimensional volume analysis (Figure 7.16). The effect of stress in the initiation stage[44] of IGC can be confirmed by comparing unstressed and 70% YS samples. With the application of stress, IGC volume loss is rapid during the initial immersion. Due to the limited number of in situ observations of each specimen under the synchrotron (4 scans on individual specimens during the span of almost two days), it was difficult to get more information about the initiation stage. During the later stage of immersion (15h – 36 h), growth kinetics as expressed by the volume loss is similar for both the unstressed and 70% stressed samples (Figure 7.17).

It should also be noted that though the total current remains constant as a function of time during the third stage of IGC growth reported by Rota and Boehni [218], the amount of charge passed which is a direct measure of total volume loss still increases with increasing exposure time. So, in this present study it is not surprising to see that the volume loss due to IGC increases during the later stage of exposure. A significant difference in the volume loss between the 70% YS sample and 90% YS sample has been found in this study. After 35 hours of exposure, IGC volume loss in the 90% YS sample is almost one order of magnitude higher than that of the unstressed or 70% YS sample.

[44] Effect of applied stress on the initiation of localized corrosion is discussed in Chapter 6. It was found that applied stress equivalent of 70% YS or more had an adverse effect on the corrosion properties of AA2024-T351.

The exact reason for this significant increase in the volume loss for a sample stressed to 90% of its yield strength is not properly understood as yet. But it is possible that once the microstructure is weakened by the IGC growth, the grains starts to slide apart more rapidly in a 90% YS sample (as it is very closed to the plastic domain of the material) than in a unstressed or in a 70% YS sample. These kinds of sliding will open up the grains along their edges and once these grain edges coalesce, IGC propagates through the microstructure. It is also possible that the specimen stressed to 90% YS starts off with many more initiation sites compared to the unstressed or 70% YS specimens. Higher number of such initiation sites would contribute to the higher volume of material loss in the later stage.

As it has already been discussed in Chapter 6,[45] during potentiostatic polarization of AA2024-T351 in aerated 0.01 M NaCl in the anodic region (between OCP and the breakdown potential), the difference in the charge passed (which is directly proportional to the metal dissolution) between an unstressed sample and a sample stressed to 45% of its yield strength is negligible (see Figure 6.34 in Chapter 6). When the sample is stressed to 70% of its yield strength, slight increase in the passed charge occurs (see Figure 6.37 in Chapter 6) and when the applied stress is 90% of the yield strength, charge passed for stressed sample is always much higher in comparison to the unstressed sample (see Figure 6.40 in Chapter 6). This possibly emphasizes the fact that, microstructural changes in a sample could happen close to its yield strength, and this might have an adverse effect on corrosion susceptibility.

Application of stress is found to decrease the initiation time for localized corrosion in stainless steel without increasing the number of nucleation sites significantly

[45] See Chapter 6 to find out more about the effect of elastic and plastic stress on the localized corrosion of aluminium alloys.

[322]. Application of stress is believed to generate surface defects such as slip lines, slip bands, microcracks, decohesion between phases [29, 35, 36, 323, 324]. All these surface defects may act as potential sites for corrosion initiation. However, individual contribution from each of these defects or possible synergistic effects of more than one factor still remains a subject of further investigations.

7.5 Conclusions

1. X-ray synchrotron tomography is a powerful non-destructive technique which can be used to visualize, monitor, and quantify real time corrosion development in three dimensions within the bulk of a material in micron and submicron scale. This technique has been shown to be an effective tool for better understanding of the electrochemical and physical mechanisms responsible for the development as well as propagation of localized corrosion sites (i.e., intergranular corrosion in this case) in aluminium alloys.
2. Quantitative growth rates of intergranular corrosion along with their morphological evolution in unstressed and stressed condition provide valuable input that can have significant contribution in the life prediction modelling tool of the aircraft components.
3. This current study documents the effect of stress on the growth rate of intergranular corrosion for the first time in three dimensions. It has been shown that 2D technique may not always quantify the growth rate accurately as localized corrosion propagation can stop in a particular direction but still continuing growth

in other directions. Under these circumstances, 3D analysis has been seen to provide a better description of the corrosion process.

4. Application of stress of 70% YS or above has a significant effect on the localized corrosion propagation of the sample. Increase in the remotely applied stress increased the amount of attack.
5. All attacks were intergranular corrosion in nature, no cracking was observed even after long exposure in this particular environment. 3D reconstruction provides the visual evidence as to how IGC propagates in three dimensions.
6. Growth of the IGC attacks in the L direction stop after certain time in most of the samples.
7. A linear relationship between the volume loss due to IGC and exposure time has been observed in both stressed and unstressed sample. Sample stressed to 90% of its yield strength showed rapid increase in the volume loss due to IGC with increasing immersion time and resulting volume loss was almost 30% of the total sample volume.

8 OVERALL SUMMARY AND CONCLUSIONS

In this project, efforts have been made to gain a better understanding of the role of intermetallic particles and applied stress in initiating and propagating localized corrosion (mainly pitting and intergranular corrosion) in aluminium alloy 2024 (Al-Cu-Mg). The initiation stage of the localized corrosion was investigated using macro and micro-scale electrochemical techniques whereas propagation of localized corrosion was studied with X-ray synchrotron tomographic techniques.

8.1 Effect of Stress on Localized Corrosion Initiation

In earlier studies by other researchers (in unstressed conditions), initiation of localized corrosion in aluminium alloys has been associated with the presence of intermetallic particles on the alloy surface [8-11, 14, 15, 37, 38, 40, 42, 47, 48, 82, 123, 171, 173, 175, 181-197]. However, the role of those intermetallic particles in initiating localized corrosion has not been well studied under stressing conditions. It has also not been well documented whether morphological changes in the intermetallic particles play any key role in controlling the corrosion properties of the alloy under stress.

The role of applied stress in the initiation of localized corrosion was investigated with a special emphasis on the behaviour of intermetallic particles under stress. Application of plastic stress on AA2024-T351 was found to decrease the corrosion and breakdown potentials of the alloy. It has been seen in this study that application of stress creates delamination at the intermetallic particle/matrix interface. Presence of any

micro/nano crevices (which could be produced by particle/matrix delamination during application of stress) at the particle edge are thought to decrease the breakdown potential of the alloy by increasing the electrochemical reactivity at those tight creviced areas.

It should be noted that most of the particles do not show any delamination even at a high plastic load (equivalent to 140% of the yield strength of AA2024-T351). However, due to the presence of a large number of intermetallic particles in AA2024-T351, the likelihood of exposing such a flaw is high even with a very small exposure area. Since the localized corrosion properties of an alloy could be determined even by a single weak point, it is highly probably that the exposed area of even one mm diameter would contain such delaminated areas. In a few cases during the current study, the application of plastic stress does not change the breakdown potential of the AA2024-T351 specimens. These observations are probably indicative of the fact that the corrosion performance of the alloy might be controlled by the probability of the existence of delamination at the particle/matrix interface in the exposed areas. Electrochemical experiments on the surface treated AA2024-T351 samples (i.e., without 'S' phase particles) do not show total elimination of the stress effect (as the breakdown potential of the alloy is still lowered by the application of plastic stress). These observations emphasize the fact that the presence of intermetallic particles other than 'S' phase particles could also play a role in determining the corrosion behaviour of the alloy under stressing condition.

Further electrochemical experiments with an intermetallic particle free Al-0.099Cu binary alloy also points out at the possible crucial role of the presence of intermetallic particle under stressing conditions. The binary alloy (Al-0.099Cu) without any intermetallic particles does not show any drop in breakdown potential after application of plastic stress though it does show drop in corrosion potential. The plastically stressed intermetallic particle free Al-0.099Cu binary alloy shows the presence

of slip lines/bands and related microcracks on the alloy surface and these features are seen to interact with the electrolyte during the corrosion experiments. However, the absence of any change in the breakdown potential of the plastically stressed Al-0.099Cu binary alloy during the corrosion experiment indicates that in the absence of intermetallic particles, the slip bands or rough surface may not be the main responsible features in changing the breakdown potential of the alloy.

The importance of the delamination at the particle/matrix interface as the possible key controlling factor on localized corrosion initiation in AA2024-T351 has further been emphasized by the experimental results from micro-capillary electrochemical tests. It has been found that application of plastic stress close to the ultimate tensile strength of the alloy does not significantly change the corrosion behaviour of the particle free matrix. The results also indicate that in the absence of a delamination at the particle/matrix interface, plastically stressed Fe-Mn rich particles do not exhibit any change in the breakdown potential.

Since it seems that formation of a tight crevice at the particle/matrix interface can potentially control the localized corrosion initiation, it is logical to assume that any process that minimises the possibility of a tight crevice formation could actually increase the breakdown potential. This argument could possibly be supported by the observed higher breakdown potentials of the Fe-Mn particles with longer cathodic polarization during the micro-capillary electrochemical experiments. Longer duration of the cathodic polarization will generate more alkalinity which may create alkaline grooving around the particles. These relatively wider grooves can alter the geometry of tight crevices and thereby minimize the chance of initiating pits. Presence of such alkaline grooving around the particles was verified through optical profilometry and AFM analysis in this current study.

8.2 Effect of Stress on Localized Corrosion Propagation

As in most of the practical applications, aluminium alloys are subjected to stress in order to achieve a specific structure; researchers try to understand the effect of stress on the growth kinetics of localized corrosion. Inherent limitations of the two dimensional techniques that are used to investigate the anisotropic growth rate of localized corrosion in aluminium alloys impose difficulties in knowing the actual growth rate in a real bulk material in three dimensions. Two dimensional analysis of the corrosion growth also do not provide any information about the true shape, connectivity, and morphology of corrosion sites along with their interactions with different microstructural features.

This current study emphasizes that X-ray synchrotron tomography can be used to visualize and characterize the development and growth of localized corrosion quite accurately in three dimensions. Hence, it is demonstrated here that X-ray synchrotron tomography can overcome the limitations associated with the conventional two dimensional techniques. This study also establishes the effect of applied stress on localized corrosion (predominantly intergranular corrosion) propagation in aluminium alloys. It has been found that application of stress of 70% Y.S. or above has a significant effect on the localized corrosion propagation within the sample. An increase in the applied stress increases the amount of attack. All attack sites are found to be intergranular in nature and no cracking is observed even after long exposure in the environment of naturally aerated 0.6M NaCl at room temperature.

3D reconstruction and rendering of X-ray attenuation data visually represents the propagation of intergranular corrosion in three dimensions. The propagation rate of the intergranular attack is found to be faster in the rolling (L) and in transverse (stressing)

direction compared with the short transverse direction. In the short transverse (S) direction, the growth rate was slower probably because of the longer path around the grains in that direction. It is interesting to note that using two dimensional techniques, several researchers found the intergranular corrosion growth to follow a t^n penetration relationship which is represented as $d = Kt^n$, where d is the depth of penetration, K is a constant, t is time and n is a fraction between 0 and 1 [29, 55, 319, 320]. However, in this current study, representing the growth rate of intergranular corrosion as the volume of material loss as a function of exposure time, a linear relationship has been observed in both stressed and unstressed samples. A sample stressed to 90% of its yield strength shows a rapid increase in the volume loss due to intergranular corrosion with increasing immersion time and results in almost 30% loss of the total sample volume. Thus, this current study shows the effect of stress on the growth kinetics of localized corrosion in three dimensions for the first time in aluminium alloys.

9 FUTURE WORK

Modelling of corrosion of aluminium alloys has become a subject of great interest to the aircraft manufacturers and maintainers during the last decade or so. Fundamental understanding of the corrosion initiation process in aluminium alloys will be helpful to develop better mitigation strategies and inspection schedules. Moreover, techniques which provide better insights and subsequent model inputs into the growth kinetics of localized corrosion will enhance the success of these predictive models with higher accuracy.

Different theories have been proposed to explain the effect of stress in changing the corrosion and breakdown potentials in aluminium alloys, but none are complete on their own. Moreover, very limited research has been carried out on the intermetallic particle behaviour under applied stress and its subsequent influence on corrosion properties. In this work, experimental evidence has been found which indicates that delamination at the particle/matrix interface can provide corrosion initiation sites by creating nano/microcrevices. However, considering the fact that delamination does not occur in all the particles and AA2024 has about 300,000 particles in every inch square, statistics seems to play a significant role in characterizing the localized corrosion initiation. Hence, some statistical studies should be performed to calculate the percentage of particle delamination and the probability of delamination for a given surface area and then correlate these calculations with observed corrosion behaviour.

Micro-capillary electrochemical cell testing in conjunction with the stressing stage provides a good opportunity to extend the statistical based study on individual intermetallic particles of AA2024-T351. Further micro-capillary electrochemical

experiments can be performed on additional (i.e., on the order of 100 to 1000 for statistical significance) individual particles under stressing condition to get quantitative evidence for the delamination-induced localized corrosion initiation theory. These experiments can also be used to understand the role of elastic and plastic stress in controlling the corrosion properties in aluminium alloys. It is also possible to expand these test matrixes to other alloy systems used in structural components for better understanding of the local electrochemical behaviour of second phase particles, inclusions etc. in both stressed and unstressed condition.

The latest generation of X-ray synchrotron microtomography beam lines have been shown to be very powerful tools to the materials and corrosion scientists. 3D information characterising localized corrosion has been obtained from the bulk of the material using this non destructive technique. Growth kinetics has been measured as a function of material loss in both unstressed and stressed samples. However, additional experiments should be performed to provide additional data for a better and accurate understanding of the growth rates. It has to be mentioned that, due to the lack of beam line time, experiments could only be performed on single specimens in the unstressed condition and in specimen stressed to 70% and 90% Y.S. Though this current study can be taken as a proof of concept demonstration showing the possibility of getting new information using X-ray synchrotron tomography, the results obtained from this study should be verified with repeat experiments to ensure consistency. The growth law obtained utilising the total volume percent of corroded material as the metric for growth rate should also be verified with repeat experiments in both stressed and unstressed samples. Moreover, due to the capabilities of the current synchrotron facilities, gaps exist in the recorded evolution of the localized corrosion events as attack occurs between two consecutive tomographic scans. Hence, more experiments with shorter intervals between

two consecutive scans should be performed utilising the newest synchrotron technology and thereby enhancing the chance of detecting the corrosion initiation and documenting the propagation phenomena more accurately.

As the scientists on the X-ray synchrotron beam-line improve the resolution of the tomographic scans, the ability to perform in situ localized corrosion tests with higher resolution (i.e., in sub micron level) on the aluminium alloys in both stressed and unstressed conditions would be recommended. These experiments would help to get statistical data on the particle delamination. Micro-capillary electrochemical tests could also be performed in conjunction with stressing stage under the synchrotron beam. Faster scan rate and high resolution of X-ray synchrotron technique can make it possible to directly correlate the localized corrosion initiation phenomena with responsible microstructural features.

APPENDIX A: MECHANISMS AND MODELS FOR PIT INITIATION

A.1 Adsorption Mechanism

Adsorption mechanism for pitting corrosion initiation is based on the reversible competitive adsorption of aggressive ions like Cl^- with oxygen for sites on the metal or alloy surface [18, 112, 129, 130, 135, 155]. Pits develop at sites where passivating oxygen adsorbed on the metal surface is displaced by aggressive anions like halides. The adsorbed halides induce pitting by weakening the metal ions to metal lattice bond or by thinning the passivating oxide film [134].

Hoar *et al.* [135] proposed that halide ions gets adsorbed on the oxide film of the surface and form traditional complexes which will immediately separate from the oxide ions in the lattice and dissolve in the solution. The rate of dissolution of the cations in the form of a complex is much higher than the non or aquo-complexed cations present in the film surface in the absence of halide ions. Once a cation is dissolved in the solution, another cation comes through the film to replace the dissolved cation. However, after reaching the film/solution interface the cation does not find any stabilizing oxide ion, rather it finds several halide ions. Hence, once begun, this process has a strong probability to be 'catalytic' in nature and thereby causing localized breakdown of the film. Apart from halide ions, depending on the size and charge of the ions, other ions may also penetrate the passive oxide by contaminating it and making it a better ionic conductor. However, according to Hoar's adsorption model, anions other than Cl^-, e.g. SO_4^{2-}, ClO_4^{2-}, NO_3^-, OH^- should also accelerate pitting by contaminating the oxide film. However, it is

found that SO_4^{2-}etc. is inhibitor to the pitting attack. Inhibition even found to occur at potential where pitting would normally occurs in the absence of those ions.

So, to explain these discrepancies, Leckie and Uhlig [130] proposed an alternate model based on the competitive adsorption of the oxygen and chloride ions. Adsorbed oxygen rather than metal oxide is considered to make up the passive film. When O^{2-} is adsorbed, the metal passivates whereas adsorption of chlorides does not produce a passive surface. Thus, above a critical potential where Cl^- adsorption is favoured over O^{2-} adsorption, localized breakdown of the passivity occurs. When anions other than Cl^- are present, these also tend to adsorb on the passive metal/alloy surface displacing the Cl^-. Hence, in the presence of these ions, the competitive process requires a shift of potential to still more noble values where Cl^- concentration in the double layer would be adequate to displace the oxygen from the passive film and thereby destroying the local passivity [130].

The aspects of the adsorption model are still relevant, though it is now known that the passive film is at least several mono layers thick rather than just an adsorbed oxygen layer [112]. It has been found that chloride and other halides can cause thinning of the passive film even under condition where as pit had not formed.

A.2 Penetration Mechanism

According to this mechanism, aggressive anions such as Cl^- incorporate into the passive film and migrate through it. Breakdown of passivity occurs when the aggressive anion reaches the underlying metal [18, 112, 128, 132, 137]. Migration of anion through the passive film would be assisted by the presence of high electric field in the film.

The existence of an induction time prior to the pitting process supports the idea behind the penetration mechanism. However, it should be noted that the theoretically calculated time for Cl^- penetration through the oxide film is much longer than the induction time measured experimentally. A critical concentration of chloride in the inner oxide portion is thought to be associated with film breakdown and pit initiation [112, 155].

Penetration models could be divided into two broad categories: (i) according to this type, penetration of chlorides occurs through the imperfections in the passive film, and (ii) in the second type, penetration is believed to occur with some interaction of chloride with the oxide lattice [18].

According to Hoar *et al.* [325] anions enter the oxide film under the influence of an electrostatic field across the film/solution interface. Initiation of pit occurs when the field reaches a critical value corresponding to the breakdown potential. Presence of imperfections (e.g., grain boundaries) in the passive film makes the entrance of the aggressive anions much easier. Efficiency of those anions in breakdown depends on their respective ease of entrance through the passive film. The smaller anions like Cl^- penetrate more readily and hence more aggressive than the Br^- and I^-. It is also suspected that oxide film 'contaminated' with aggressive anions are better ionic conductor than the original passivating oxide [325].

McCafferty [120] supported the second type of penetration model where it is considered that penetration of chloride ions can occur through the oxide film dissolution. According to this model chloride ion gets adsorbed on the oxide surface, mostly on the positively charged region of the surface. This model has been extended in such a way that the anion penetration through the oxide film could be explained by oxide film dissolution as well as by migration through the oxygen vacancies.

On the other hand, Mattin and Burstein [326, 327] proposed a model where both chloride and oxide ions are suggested to be drawn through the passivating oxide film under the influence of a high electric field. Oxide ions react at the metal/film interface to form passivating metal oxide, whereas chloride form metal chloride after reaching at that interface. Formation of solid metal chloride at that interface would expand the interface because of the higher molar volume of the metal chlorides than the metal oxide or the metal itself. This expansion causes mechanical rupture of the oxide film leading to a microscopic explosion which could be the precursor of the pit nucleation [18].

A.3 Film Breakdown Mechanism

Pit initiation by film breakdown considers that the thin passive film is in a continual state of breakdown and repair [18, 112, 137]. This model assumes the existence of competition between film formation and metal dissolution. Pitting thought to occur at potentials where the rate of passivity breakdown is greater than that of repassivation [134]. According to Smialowska [18] the film breakdown mechanism (also termed as "depassivation-repassivation" theory) is a modification of adsorption-displacement theory of competitive adsorption between Cl^- and O^{2-} on the metal surface. In this theory of pit initiation, breakdown potential (E_p) is referred a particular potential at which the adsorption of aggressive anions on the metal surface displaces the adsorbed passivating species.

Mechanical stresses at the weak sites or flaws on the oxide film resulting from the electrostriction and surface tension can lead into the local breakdown of the passive film [112]. However, in a non-aggressive environment (i.e., in the absence of chloride or other

aggressive anions) the passive film can reform very rapidly. By comparison, the likelihood of the film reform will decrease rapidly in the presence of aggressive anions and sufficiently high potential. As a result the metal surface at those defective sites becomes activated and attacked by the formation of soluble non protective corrosion products. In this model, the role of chloride ions is restricted to prevent repassivation rather than promoting breakdown [18].

While considering this film breakdown mechanism, it should be remembered that not all the breakdown events would result into pitting corrosion. According to this model, breakdown will only lead to pitting corrosions where pit growth is possible [112]. It is assumed that breakdown will always occur, but the passive film properties will influence the rate of its occurrence.

Pit stability criteria play an important role in describing the pitting corrosion mechanism using this model. According to this model, film breakdown occurs probably with a different energy and at different spots on the film. Hence, there is a need to establish some criteria that can describe the conditions needed pit to be able to grow. Hence several researchers [114] suggested a critical factor for pit stability mainly consisting of the product of pit depth and pit current density [112]. If the product (which could be different for different metals/alloys) of this exceeds a certain value, pit is supposed to be stable. So, it can be stated as summary that the film breaking model really involves initiation based on pit growth stability [112].

A.4 Mechano - Chemical Model

This model/mechanism of pit initiation describes with the interaction between the aggressive anions with the passive oxide film which could be under mechanically stressed condition [18, 128, 133, 134, 328]. Mechanical stress in the anodic oxide film can arise due to the reasons like: (i) interfacial tension, (ii) electrostriction pressure resulting from the presence of a high electric field in the film, (iii) internal stress caused by the volume ratio of the film and the metal, (iv) internal stress due to partial hydration or dehydration of the film, or (iv) local stresses caused by the impurities. Under these operating stresses, surface tension probably stabilizes the anodic oxide film. However, this surface tension effect decreases with the increase in the film thickness and this will lead to the existence of a critical film thickness above which breakdown of the passive film could occur. Adsorption of the aggressive anions on the oxide film will lower the surface tension and hence decrease the critical thickness for breakdown [133]. Thus breakdown potential at the critical film thickness is found to depend on the anion concentration in the solution [133]. Hoar [328] suggested that the adsorption of Cl^- onto the film/solution interface results in “peptization” due to the mutual repulsion of the adsorbed charged species. When the repulsive forces are sufficiently high, the film cracks. Sato [133] suggested that nature of oxide film breakdown depends on the mechanical properties of the film. Rigid anhydrous metal oxide would result into brittle crack or fracture whereas visco-plasctic hydrous oxide would result into plastic deformation or flow. Sato [133] suspected that in case of plastic flow continuous breakdown can proceed by producing pores on top of the anodic oxide film. However, any of these types of damages (i.e., either flaws or pores) in the anodic oxide film would expose the underlying metal for dissolution.

A.5 Point Defect Model for Pit Initiation

Point defect model for pit initiation can also be correlated with the penetration mechanism as described earlier [112]. In the point defect model, a passive film is regarded as containing numerous point defects [18, 112, 154-156]. The major point defects in an oxide film are assumed to be electron, and metal (cation) and oxygen (anion) vacancies. Metal and oxide vacancies are in their equilibrium states at the metal/solution and film/solution interface. Film thickening occurs when anion diffuses from the film/solution interface to the metal/film interface. On the other hand cation diffusion results only in dissolution.

Metal vacancies (or "metal holes") are created at the metal/film interface due to the diffusion of cation from the metal/film to the film/solution interfaces. These "metal holes" will tend to submerge into the bulk of the metal and hence to "disappear" [155]. However, when the cation diffusion rate (i.e., the "metal hole" production rate) is higher than the rate of "metal hole" submerge into the bulk, the metal holes start pilling up and hence will form a void at the metal/film interface (this is the process of pit incubation). When the void grow to a certain critical size, the passive film suffer local collapse and thereby initiating pitting corrosion [18, 155].

Cl^- ions are capable of being incorporated into passive film through the occupation of oxygen vacancies by the Cl^- ions. In order to main the charge neutrality, the number of vacant cation sites in the neighbourhood must increase [156]. In this mechanism, anion absorption increases the generation of cation vacancies across the barrier layer. Thus, though the generation of cation vacancies is autocatalytic, but whether or not the film breaks down depend on the relative rates with which the cation vacancies are transferred across the barrier layer and are annihilated by emissions of cations from the metal into the

film. Passivity breakdown is though to occur at regions of the film that are characterized by high cation vacancy diffusivities [156].

A.6 Localized Acidification Theory

Galvele [114] was the first to propose the "localized acidification mechanism" where the induction time for pitting is described as the time required to achieve the critical pH inside the pit initiation sites. It is also suggested that pit develops because of the hydrolysis of corrosion products during transient cracks in the oxide film thus causing acidification at the metal surface [134]. On the other hand, Smialowska [18] treated this model as a "pit growth" model than "pit initiation" model. According to Smialowska [18] pits can be formed only when the passive film if destroyed locally; however subsequent pit growth will be determined by the formation of a pit solution that prevents the repassivation.

Galvele [114] assumed that film breakdown occurs constantly even below the pitting potential. In the presence of high enough electrode potential, a crack in the passive film will promote metal dissolution followed by a hydrolysis reaction which will drop the pH inside the pit. Galvele suggested that for each metal and alloy, a critical acidification is necessary to render repassivation impossible and sustain pit activity. The pitting potential does not have any special thermodynamic significance according to this model; rather it is described as a potential necessary to reach the current density for the critical x.i (i.e., pit depth.current density) [18].

Galvele [114] found that in most of the metals the critical pH is reached with x.i values lower than 10^{-6} A/cm. Since at pit initiation conditions the current density the pit is

at least $1A/cm^2$, it is concluded that the necessary acidification can be obtained in pits as small as 10^{-6} cm. This means that a crack in the passivating oxide film would give a diffusion path long enough to reach the critical pH. If such cracks are present, it would only be necessary to apply potential high enough to reach the above mentioned current density.

Thus, Galvele's model is based on the dissolution of a metal, cation hydrolysis, diffusion and migration, which leads to the prediction of pit acidification.

A.7 Chemical Dissolution Theories

According to the theories aggressive anions and metal ions in oxide film form complexes that cause localized thinning of the film leading to its breakdown [120, 135, 139, 155, 157]. The chemical dissolution theory suggests that small number of Cl^- ions jointly adsorbed around a cation in the film surface to form a high energy complex and once formed, this complex will readily dissolve into the solution making the oxide film thinner locally. The presence of a stronger anodic field at this site will rapidly transfer another cation to the surface where it will meet more Cl^-, complex with them, and thereby enter the solution. Thus this process will become auto-catalytic and results in film thinning [135, 155].

Nguyen and Foley [107, 139] have performed extensive study on the chemical nature of aluminium corrosion. Nguyen experimental results support the idea that the first steps in aluminium pitting in aggressive solutions involve adsorption of the anion on the oxide film followed by chemical interaction to form a soluble species resulting in a thinning of the film and direct contact with the metal surface.

According to Foley's group the initiation of pitting of aluminium in halide solutions proceeds in four consecutive steps:

i) Adsorption of the aggressive anion on the oxide film

ii) The chemical reaction of the adsorbed anion with the Al^{3+} in the oxide lattice:

$$Al^{3+}(in Al_2O_3.nH_2O lattice) + Cl^- \rightarrow Al(OH)_2Cl$$

iii) The thinning of the oxide film by dissolution

iv) The direct attack of the exposed metal by the aggressive anion with the formation of transient complexes which rapidly undergo hydrolysis:

$$Al^{3+} + 4Cl^- \rightarrow AlCl_4^-$$

$$AlCl_4^- + 2H_2O \rightarrow Al(OH)_2Cl + 2H^+ + 3Cl^-$$

REFERENCES

1. E. Ghali, in *Uhlig's Corrosion Handbook*, R. W. Revie (Editor), John Wiley & Sons, p. 677, 2000.
2. J. G. Kaufman, in *Handbook of Materials Selection*, M. Kutz (Editor), John Wiley & Sons, Inc., New York, 2002.
3. N. P. Cheremisinoff, *Materials Selection Deskbook*, William Andrew Publishing, 1996.
4. E. A. Starke, Jr., and J. T. Staley, *Progress in Aerospace Sciences*, **32**(2-3), 131-172, 1996.
5. I. J. Polmear, *Light Alloys - Metallurgy of the Light Metals*, Arnold, London, 1995.
6. P. Campestrini, E. P. M. van Westing, H. W. van Rooijen, and J. H. W. de Wit, *Corrosion Science*, **42**(11), 1853-1861, 2000.
7. V. Guillaumin, and G. Mankowski, *Corrosion Science*, **41**(3), 421-438, 1999.
8. G. S. Chen, M. Gao, and R. P. Wei, *Corrosion*, **52**(1), 8-15, 1996.
9. R. G. Buchheit, R. P. Grant, P. F. Hlava, B. Mckenzie, and G. L. Zender, *Journal of the Electrochemical Society*, **144**(8), 2621-2628, 1997.
10. Y. Yoon, and R. G. Buchheit, *Journal of the Electrochemical Society*, **153**(5), 151-155, 2006.
11. C. M. Liao, J. M. Olive, M. Gao, and R. P. Wei, *Corrosion*, **54**(6), 451-458, 1998.
12. M. Shao, Y. Fu, R. Hu, and C. Lin, *Materials Science and Engineering A*, **344**(1-2), 323-327, 2003.
13. Z. Liu, P. H. Chong, A. N. Butt, P. Skeldon, and G. E. Thompson, *Applied Surface Science*, **247**(1-4), 294-299, 2005.
14. R. G. Buchheit, L. P. Montes, M. A. Martinez, J. Michael, and P. F. Hlava, *Journal of the Electrochemical Society*, **146**(12), 4424-4428, 1999.
15. J. F. Li, Z. Ziqiao, J. Na, and T. Chengyu, *Materials Chemistry and Physics*, **91**(2-3), 325-329, 2005.
16. T. Suter, and H. Bohni, *Electrochimica Acta*, **42**(20-22), 3275-3280, 1997.
17. T. Suter, and H. Bohni, in *Analytical Methods in Corrosion Science and Engineering*, P. Marcus and F. Mansfeld (Editors), Taylor & Francis Group, London, p. 649-696, 2006.
18. Z. Szklarska-Smialowska, *Pitting and Crevice Corrosion*, NACE International, Houston, Texas, 2005.
19. F. Moulinier, "*Effects of a Surface Treatment on the Corrosion and Fatigue Behaviour of a High Strength Aluminium Alloy*", University of Birmingham, PhD Thesis, 2003.
20. C. M. Rangell, M. H. Simplicio, and M. G. S. Ferreira, *British Corrosion Journal*, **27**, 237, 1992.
21. E. M. Gutman, G. Solovioff, and D. Eliezer, *Corrosion Science*, **38**(7), 1141-1145, 1996.
22. T. P. Hoar, and F. P. Ford, *Journal of the Electrochemical Society*, **120**(8), 1013-1019, 1973.
23. F. Navai, and O. Debbouz, *Journal of Materials Science*, **34**, 1073, 1999.

24. V. Vignal, C. Valot, R. Oltra, M. Verneau, and L. Condreusse, *Corrosion Science*, **44**, 1477, 2002.
25. G. Bombara, *Corrosion Science*, **19**(12), 991-999, 1979.
26. P. Peyre, X. Scherpereel, L. Berthe, C. Carboni, R. Fabbro, G. Beranger, and C. Lemaitre, *Materials Science and Engineering A*, **A280**, 294, 2000.
27. F. Navai, *Journal of Materials Science*, **35**, 5921-5925, 2000.
28. T. Suter, E. G. Webb, H. Bohni, and R. C. Alkire, *Journal of the Electrochemical Society*, **148**(5), B174-B185, 2001.
29. X. Liu, G. S. Frankel, B. Zoofan, and S. I. Rokhlin, *Corrosion Science*, **46**(2), 405-425, 2004.
30. V. Vignal, R. Oltra, and C. Josse, *Scripta Materialia*, **49**, 779-784, 2003.
31. R. Oltra, and V. Vignal, *Corrosion Science*, **49**(1), 158-165, 2007.
32. V. Vignal, N. Mary, R. Oltra, and J. Peultier, *Journal of the Electrochemical Society*, **153**(9), B352-B357, 2006.
33. V. Vignal, N. Mary, C. Valot, R. Oltra, and L. Coudreuse, *Electrochemical and Solid-State Letters*, **7**(4), 39-42, 2004.
34. D. Chastell, P. Doig, P. E. J. Flewitt, and K. Ryan, *Corrosion Science*, **19**(5), 335-341, 1979.
35. Z. Zhao, and G. S. Frankel, "The Effects of Prior Deformation on Localized Corrosion of Al Alloys," The Ohio State University Research Foundation, Columbus, OH, 2005.
36. B. J. Connolly, in *Local Probe Techniques in Corrosion Research*, R. Oltra (Editor), Woodhead Publishing Limited, Cambridge, UK, p. 155-166, 2007.
37. G. O. Ilevbare, O. Schneider, R. G. Kelly, and J. R. Scully, *Journal of the Electrochemical Society*, **151**(8), 453-464, 2004.
38. O. Schneider, G. O. Ilevbare, J. R. Scully, and R. G. Kelly, *Journal of the Electrochemical Society*, **151**(8), 465-472, 2004.
39. T. Suter, and R. C. Alkire, Critical Factors in Localized Corrosion III, Electrochemical Society, p. 118-129, 1998.
40. T. Suter, and R. C. Alkire, *Journal of the Electrochemical Society*, **148**(1), B36-B42, 2001.
41. F. Andreatta, M. M. Lohrengel, H. Terryn, and J. H. W. de Wit, *Electrochimica Acta*, **48**(20-22), 3239-3247, 2003.
42. N. Birbilis, and R. G. Buchheit, *Journal of the Electrochemical Society*, **152**(4), B140-B151, 2005.
43. P. Schmutz, and G. S. Frankel, *Journal of the Electrochemical Society*, **145**(7), 2295-2306, 1998.
44. P. Schmutz, and G. S. Frankel, *Journal of the Electrochemical Society*, **145**(7), 2285-2295, 1998.
45. T. J. Warner, M. P. Schmidt, F. Sommer, and D. Bellot, *Zeitschrift fur Metallkunde*, **86**(7), 494-501, 1995.
46. P. Leblanc, and G. S. Frankel, *Journal of the Electrochemical Society*, **149**(6), 239-247, 2002.
47. R. M. Rynders, C. H. Paik, R. Ke, and R. C. Alkire, *Journal of the Electrochemical Society*, **141**(6), 1439-1445, 1994.
48. J. O. Park, C. H. Paik, Y. H. Huang, and R. C. Alkire, *Journal of the Electrochemical Society*, **146**(2), 517-523, 1999.
49. F. Hunkeler, and H. Bohni, *Corrosion*, **37**(11), 645-650, 1981.
50. F. Hunkeler, and H. Bohni, *Corrosion*, **40**(10), 534-540, 1984.

51. A. Sehgal, G. S. Frankel, B. Zoofan, and S. Rokhlin, *Journal of the Electrochemical Society*, **147**(1), 140-148, 2000.
52. W. Zhang, and G. S. Frankel, *Journal of the Electrochemical Society*, **149**(11), 510-519, 2002.
53. X. Liu, G. S. Frankel, B. Zoofan, and S. I. Rokhlin, *Corrosion Science*, **49**(1), 139-148, 2007.
54. X. Liu, G. S. Frankel, B. Zoofan, and S. I. Rokhlin, *Corrosion*, **62**(3), 217-230, 2006.
55. X. Zhao, G. S. Frankel, B. Zoofan, and S. I. Rokhlin, *Corrosion*, **59**(11), 1012-1018, 2003.
56. *ASM Speciality Handbook: Aluminum and Aluminum Alloys*, ASM International, Ohio, 1993.
57. C. R. Brooks, *Heat Treatment, Structure and Properties of Nonferrous Alloys*, American Society for Metals, Ohio, 1990.
58. J. B. Dwight, *Aluminum Design and Construction*, Spon Press, UK, 1999.
59. *Smithells Metals Reference Book*, Butterworth Heinemann, Oxford, 2004.
60. G. E. Dieter, *Mechanical Metallurgy*, McGraw-Hill, New York, 1986.
61. J. T. Staley, in *Aluminum Alloys - Contemporary Reserach and Applications*, A. K. Vasudevan and R. D. Doherty (Editors), Academic Press, Inc., New York, 1989.
62. K. R. Van Horn, *Aluminum, Vol. I: Properties, Physical Metallurgy, and Phase Diagrams*, ASM, Metal Park, Ohio, 1967.
63. L. F. Mondolfo, *Aluminium Alloys: Structures and Properties*, Butterworth & Co, London, 1976.
64. *Properties of Wrought Aluminium and Aluminium Alloys, Metals Handbook, Properties and Selection: Nonferrous Alloys and Special Purpose Materials*, vol. 2, ASM International, Material Park, Ohio, 1990.
65. *ASM Handbook, Heat Treating*, vol. 4, ASM International, Material Park, Ohio, 1991.
66. M. Nakai, and T. Eto, *Materials Science and Engineering A*, **285**(1-2), 62-68, 2000.
67. G. T. Hahn, and A. R. Rosenfield, *Metallurgical Transactions A (Physical Metallurgy and Materials Science)*, **6A**(4), 653-668, 1975.
68. S. Suresh, *Fatigue of Materials*, Cambridge University Press, Cambridge, 1998.
69. D. Sigler, M. C. Montpetit, and W. L. Haworth, *Metallurgical Transactions A (Physical Metallurgy and Materials Science)*, **14A**(5), 931-938, 1983.
70. M. Jariyaboon, "*Corrosion of Friction Stir Welds in High Strength Aluminium Alloys*", University of Birmingham, PhD Thesis, 2006.
71. MatWeb - Material Property Data, 2007: *http://www.matweb.com*.
72. R. H. Brown, and L. A. Willey, in *Aluminium : Properties, Physical Metallurgy and Phase Diagrams*, K. R. V. Horn (Editor), Americal Society for Metals, Ohio, p. 53, 1967.
73. P. R. Sperry, *Transactions of the ASM*, **48**, 904-918, 1956.
74. G. O. Ilevbare, and J. R. Scully, *Journal of the Electrochemical Society*, **148**(5), 196-207, 2001.
75. M. Gao, C. R. Feng, and R. P. Wei, *Metallurgical and Materials Transactions A: Physical Metallurgy and Materials Science*, **29A**(4), 1145-1151, 1998.
76. A. E. Hughes, R. J. Taylor, K. J. H. Nelson, B. R. W. Hinton, and L. Wilson, *Materials Science and Technology*, **12**, 928-936, 1996.

77. G. O. Ilevbare, and J. R. Scully, *Corrosion*, **57**(2), 134-152, 2001.
78. M. Qian, J. A. Taylor, J. Y. Yao, M. J. Couper, and D. H. StJohn, *Journal of Light Metals*, **1**, 187-193, 2001.
79. F. King, *Aluminium and Its Alloys*, John Wiley and Sons, New York, 1987.
80. H. M. Obispo, L. E. Murr, R. M. Arrowood, and E. A. Trillo, *Journal of Materials Science*, **35**, 3479-3495, 2000.
81. E. A. DeBartolo, and B. M. Hillberry, *International Journal of Fatigue*, **20**(10), 727-735, 1998.
82. R. G. Buchheit, R. K. Boger, and M. W. Donohue, Symposium of the Seawater Corrosion, The Electrochemical Society, p. 205, 1999.
83. V. Radmilovic, R. Kilaas, U. Dahmen, and G. J. Shiflet, *Acta Materialia*, **47**(15-16), 3987-3997, 1999.
84. S. Ghosh, A. J. Davenport, and B. J. Connolly, "*Effect of Surface Treatment and S-Phase Removal on the Corrosion Properties of AA2024-T3*", *(Unpublished Work)*, University of Birmingham, 2007.
85. L. M. Wang, H. M. Flower, and T. C. Lindley, *Scripta Materialia*, **41**(4), 391-396, 1999.
86. M. E. Fine, *Metallurgical Transactions A: Physical Metallurgy and Materials Science*, **6A**(4), 625-630, 1975.
87. M. Rosen, E. Horowitz, L. Swartzendruber, S. Fick, and R. Mehrabian, *Materials Science and Engineering*, **53**(2), 191-198, 1982.
88. Y. Gefen, M. Rosen, and A. Rosen, *Material Science and Engineering*, **8**(3), 181-188, 1971.
89. N. Sen, and D. R. F. West, *Journal of the Institute of Metals*, **97**, 87-92, 1969.
90. H.-C. Shih, N.-J. Ho, and J. C. Huang, *Metallurgical and Materials Transactions A: Physical Metallurgy and Materials Science*, **27A**(9), 2479-2494, 1996.
91. A. K. Gupta, P. Gaunt, and M. C. Chaturvedi, *Philosophical Magazine A: Physics of Condensed Matter: Structure, Defects and Mechanical Properties*, **55**(3), 375-387, 1987.
92. A. K. Jena, A. K. Gupta, and M. C. Chaturvedi, *Acta Metallurgica*, **37**(3), 885-895, 1989.
93. V. Radmilovic, G. Thomas, G. J. Shiflet, and E. A. Starke, Jr., *Scripta Metallurgica*, **23**(7), 1141-1146, 1989.
94. S. P. Ringer, T. Sakurai, and I. J. Polmear, *Acta Materialia*, **45**(9), 3731-3744, 1997.
95. W. Zhang, and G. S. Frankel, *Electrochimica Acta*, **48**(9), 1193-1210, 2003.
96. in *Metals Handbook: Corrosion*, E. H. Hollingsworth and H. Y. Hunsicker (Editors), ASM International, Material Park, OH, USA, 1987.
97. J. R. Davis, *Corrosion of Aluminium and Aluminium Alloys*, ASM International, Materials Park, OH, USA, 1991.
98. M. Pourbaix, *Atlas of Electrochemical Equilibria in Aqueous Solutions*, National Association of Corrosion Engineers, Houston, Texas, 1974.
99. P. Hulser, U. A. Kruger, and F. Beck, *Corrosion Science*, **38**(1), 47-57, 1996.
100. K. C. Emregul, and A. A. Aksut, *Corrosion Science*, **42**(12), 2051-2067, 2000.
101. R. D. Armstrong, and V. J. Braham, *Corrosion Science*, **38**(9), 1463-1471, 1996.
102. S. M. Moon, and S. I. Pyun, *Corrosion Science*, **39**(2), 399-408, 1997.
103. K. Nisancioglu, The 3rd International Conference on Aluminium Alloys, Trondheim, Norway, p. 239-259, 1992.
104. E. J. Lee, and S. I. Pyun, *Corrosion Science*, **37**(1), 157-168, 1995.

105. Z. Szklarska-Smialowska, *Corrosion Science*, **41**, 1743-1767, 1999.
106. H. Bohni, in *Uhlig's Corrosion Handbook*, R. W. Revie (Editor), John Wiley & Sons, p. 173-190, 2000.
107. T. H. Nguyen, and R. T. Foley, *Journal of the Electrochemical Society*, **126**(11), 1855-1860, 1979.
108. K. Srinivasa Rao, and K. Prasad Rao, *Transactions of the Indian Institute of Metals*, **57**(6), 593-610, 2004.
109. T. Okada, *Corrosion Science*, **31**, 453-458, 1990.
110. R. T. Foley, *Corrosion (Houston, TX, United States)*, **42**(5), 277-288, 1986.
111. M. G. Fontana, *Corrosion Engineering*, McGraw-Hill Book Company, Singapore, 1987.
112. G. S. Frankel, *Journal of the Electrochemical Society*, **145**(6), 2186-2198, 1998.
113. J. R. Galvele, Critical Factors in Localized Corrosion, The Electrochemical Society, Inc, p. 94-105, 1992.
114. J. R. Galvele, *Journal of the Electrochemical Society*, **123**(4), 464-474, 1976.
115. P. L. Cabot, F. A. Centellas, J. A. Garrido, E. Perez, and H. Vidal, *Electrochimica Acta*, **36**(1), 179-187, 1991.
116. T. R. Beck, *Electrochimica Acta*, **33**(10), 1321-1327, 1988.
117. Z. Szklarska-Smialowska, *Corrosion Science*, **33**(8), 1193-1202, 1992.
118. L. Tomcsanyi, K. Varga, I. Bartik, G. Horanyi, and E. Maleczki, *Electrochimica Acta*, **34**(6), 855-859, 1989.
119. R. Ambat, and E. S. Dwarakadasa, *Journal of Applied Electrochemistry*, **24**(9), 911-916, 1994.
120. E. McCafferty, *Corrosion Science*, **45**(7), 1421-1438, 2003.
121. Z. Szklarska-Smialowska, *Pitting Corrosion of Metals*, NACE, Houston, TX, 1986.
122. K. Kowal, J. DeLuccia, J. Y. Josefowicz, C. Laird, and G. C. Farrington, *Journal of the Electrochemical Society*, **143**(8), 2471-2481, 1996.
123. R. G. Buchheit, R. K. Boger, M. C. Carroll, R. M. Leard, C. Paglia, and J. L. Searles, *JOM*, **53**(7), 29-33, 2001.
124. G. T. Burstein, L. L. Shreir, and R. A. Jarman, *Corrosion, Volume 1*, Elsevier Butterworth-Heinemann, 1994.
125. I. T. E. Fonseca, N. Lima, J. A. Rodrigues, M. I. S. Pereira, J. C. S. Salvador, and M. G. S. Ferreria, *Electrochemistry Communications*, **4**(5), 353-357, 2002.
126. D. E. Williams, J. Stewart, and P. H. Balkwill, Critical Factors in Localized Corrosion, The Electrochemical Society Softbound Proceeding Series, NJ, p. 36, 1992.
127. G. S. Frankel, L. Stockert, F. Hunkeler, and H. Bohni, *Corrosion*, **43**, 429, 1987.
128. J. Kruger, and K. Rhyne, *Nuclear and Chemical Waste Management*, **3**, 205, 1982.
129. H. Bohni, and H. H. Uhlig, *Journal of the Electrochemical Society*, **116**, 906, 1969.
130. H. P. Leckie, and H. H. Uhlig, *Journal of the Electrochemical Society*, **113**, 1262, 1966.
131. J. A. Richardson, and G. C. Wood, *Journal of the Electrochemical Society*, **10**, 313, 1970.
132. M. A. Heine, and M. J. Pryor, *Journal of the Electrochemical Society*, **114**, 1001, 1967.
133. N. Sato, *Electrochemica Acta*, **16**, 1683-1692, 1971.

134. S. T. Pride, "*Metastable pitting of aluminum and Al-Cu alloys*", The University of Virginia, PhD Thesis, 1997.
135. T. P. Hoar, and W. R. Jackob, *Nature*, **216**, 1299-1301, 1967.
136. H. H. Strehblow, in *Corrosion Mechanisms in Theory and Practice*, P. Marcus and J. Oudar (Editors), Marcel Dekker, New York, 1995.
137. J. A. Richardson, and G. C. Wood, *Corrosion Science*, **10**(5), 313-323, 1970.
138. R. T. Foley, and T. H. Nguyen, *Journal of the Electrochemical Society*, **129**(3), 464-467, 1982.
139. T. H. Nguyen, and R. T. Foley, *Journal of the Electrochemical Society*, **129**(1), 27-32, 1982.
140. M. F. Abd Rabbo, J. A. Richardson, and G. C. Wood, *Corrosion Science*, **18**(2), 117-123, 1978.
141. J. O. Bockris, and L. V. Minevski, *Journal of Electroanalytical Chemistry*, **349**(1-2), 375-414, 1993.
142. J. O. M. Bockris, and Y. Kang, *Journal of Solid State Electrochemistry*, **1**(1), 17-35, 1997.
143. P. M. Natishan, W. E. O'Grady, E. McCafferty, D. E. Ramaker, K. Pandya, and A. Russell, *Journal of the Electrochemical Society*, **146**(5), 1737-1740, 1999.
144. S. Y. Yu, W. E. O'Grady, D. E. Ramaker, and P. M. Natishan, *Journal of the Electrochemical Society*, **147**(8), 2952-2958, 2000.
145. A. Kolics, A. S. Besing, P. Baradlai, R. Haasch, and A. Wieckowski, *Journal of the Electrochemical Society*, **148**(7), 251-259, 2001.
146. M. Koudelkova, J. Augustynski, and H. Berthou, *Journal of the Electrochemical Society*, **124**(8), 1165-1168, 1977.
147. M. J. Pryor, *Corrosion Science*, **11**(6), 463-464, 1971.
148. E. J. Lee, and S. I. Pyun, *Corrosion Science*, **37**(1), 157-168, 1995.
149. J. A. Richardson, and G. C. Wood, *Journal of the Electrochemical Society*, **120**(2), 193-202, 1973.
150. B. N. Stirrup, N. A. Hampson, and I. S. Midgley, *Journal of Applied Electrochemistry*, **5**(3), 229-235, 1975.
151. Z. A. Foroulis, and M. J. Thubrikar, *Journal of the Electrochemical Society*, **122**(10), 1296-1301, 1975.
152. J. R. Galvele, and S. M. d. De Micheli, *Corrosion Science*, **10**(11), 795-807, 1970.
153. E. McCafferty, *Corrosion Science*, **37**(3), 481-492, 1995.
154. C. Y. Chao, L. F. Lin, and D. D. Macdonald, *Journal of the Electrochemical Society*, **128**(6), 1187-1194, 1981.
155. L. F. Lin, C. Y. Chao, and D. D. Macdonald, *Journal of the Electrochemical Society*, **128**(6), 1194-1198, 1981.
156. D. D. Macdonald, *Journal of the Electrochemical Society*, **139**(12), 3434-3449, 1992.
157. T. H. Nguyen, and R. T. Foley, *Journal of the Electrochemical Society*, **127**(12), 2563-2566, 1980.
158. A. R. Trueman, *Corrosion Science*, **47**(9), 2240-2256, 2005.
159. F. Sato, and R. C. Newman, *Corrosion*, **54**(12), 955-963, 1998.
160. T. T. Lunt, S. T. Pride, J. R. Scully, J. L. Hudson, and A. S. Mikhailov, *Journal of the Electrochemical Society*, **144**(5), 1620-1629, 1997.
161. B. Wu, J. R. Scully, J. L. Hudson, and A. S. Mikhailov, *Journal of the Electrochemical Society*, **144**(5), 1614-1620, 1997.

162. G. S. Frankel, L. Stockert, F. Hunkeler, and H. Boehni, *Corrosion*, **43**(7), 429-436, 1987.
163. P. C. Pistorius, and G. T. Burnstein, *Corrosion Science*, **33**(12), 1885-1897, 1992.
164. P. C. Pistorius, and G. T. Burnstein, *Corrosion Science*, **36**(3), 525-538, 1994.
165. D. E. Williams, J. Stewart, and P. H. Balkwill, *Corrosion Science*, **36**(7), 1213-1235, 1994.
166. D. W. Buzza, and R. C. Alkire, *Journal of the Electrochemical Society*, **142**(4), 1104-1111, 1995.
167. S. T. Pride, J. R. Scully, and J. L. Hudson, *Journal of the Electrochemical Society*, **141**(11), 3028-3040, 1994.
168. I. L. Muller, and J. R. Galvele, **17**(3), 179-193, 1977.
169. A. J. Davenport, "Lecture Notes - Mechanisms of Corrosion of Metals in Aqueous Environment ", 2005.
170. R. P. Wei, C.-M. Liao, and M. Gao, *Metallurgical and Materials Transactions A: Physical Metallurgy and Materials Science*, **29A**(4), 1153-1160, 1998.
171. T. J. R. Leclere, and R. C. Newman, *Journal of the Electrochemical Society*, **149**(2), B52-B56, 2002.
172. M. B. Vukmirovic, N. Vasiljevic, N. Dimitrov, and K. Sieradzki, *Journal of the Electrochemical Society*, **150**(1), B10-B15, 2003.
173. N. Dimitrov, J. A. Mann, and K. Sieradzki, *Journal of the Electrochemical Society*, **146**(1), 98-102, 1999.
174. M. A. Alodan, and W. H. Smyrl, *Journal of the Electrochemical Society*, **144**(10), L282-L284, 1997.
175. M. B. Vukmirovic, N. Dimitrov, and K. Sieradzki, *Journal of the Electrochemical Society*, **149**(9), 428-439, 2002.
176. D. A. Jones, *Principles and Prevention of Corrosion*, Macmillan Publishing Company, NY, USA, 1992.
177. H. H. Uhlig, *Corrosion Science*, **19**(11), 777-791, 1979.
178. H. H. Uhlig, and R. W. Revie, *Corrosion and Corrosion Control*, John Wiley & Sons, NY, USA, 1991.
179. C. M. Liao, and R. P. Wei, *Electrochimica Acta*, **45**(6), 881-888, 1999.
180. C. Blanc, and G. Mankowski, *Corrosion Science*, **40**(2-3), 411-429, 1998.
181. R. G. Buchheit, *Materials Science Forum*, **331 (II)**, 1641-1646, 2000.
182. R. G. Buchheit, M. A. Martinez, and L. P. Montes, *Journal of the Electrochemical Society*, **147**(1), 119-124, 2000.
183. N. Missert, J. C. Barbour, R. G. Copeland, and J. E. Mikkalson, *JOM*, **53**(7), 34-36, 2001.
184. G. Chen, M. Williams, J. Malmberg, J. S. Kim, and D. A. Buttry, Corrosion and Corrosion Prevention of Low Density Metals and Alloys - Proceedings of the International Symposium, The Electrochemical Society, p. 29-40, 2000.
185. N. Missert, R. G. Copeland, Y. Kim, and R. Buchheit, Corrosion and Protection of Light Metal Alloys, The Electrochemical Soceity, p. 55-61, 2003.
186. N. Dimitrov, J. A. Mann, M. Vukmirovic, and K. Sieradzki, *Journal of the Electrochemical Society*, **147**(9), 3283-3285, 2000.
187. J. C. Seegmiller, R. C. Bazito, and D. A. Buttry, *Electrochemical and Solid-State Letters*, **7**(1), 1-4, 2004.
188. M. Kendig, S. Jeanjaquet, R. Buchheit, H. Guan, and R. M. Leard, Corrosion and Corrosion Prevention of Low Density Metals and Alloys, The Electrochemical Society, p. 1-9, 2001.

189. A. Kolics, A. S. Besing, T. Suter, H. Bohni, C. H. Paik, R. C. Alkire, and A. Wieckowski, Corrosion and Corrosion Prevention of Low Density Metals and Alloys, The Electrochemical Society, p. 10-18, 2000.
190. R. K. Boger, and R. Buchheit, Corrosion and Corrosion Prevention of Low Density Metals and Alloys, The Electrochemical Society, p. 19-28, 2000.
191. R. G. Buchheit, *Journal of the Electrochemical Society*, **142**(11), 3994-3996, 1995.
192. Z. Szklarska-Smialowska, *Corrosion*, **27**(6), 223-233, 1971.
193. A. Kolics, A. S. Besing, T. Suter, H. Bohni, C. H. Paik, R. C. Alkire, and A. Wieckowski, Corrosion and Corrosion Prevention of Low Density Metals and Alloys, The Electrochemical Society, p. 10-18, 2001.
194. R. K. Boger, and R. Buchheit, Corrosion and Corrosion Prevention of Low Density Metals and Alloys, The Electrochemical Society, p. 19-28, 2001.
195. M. Buchler, J. Kerimo, F. Guillaume, and W. H. Smyrl, *Journal of the Electrochemical Society*, **147**(10), 3691-3699, 2000.
196. M. Buchler, T. Watari, and W. H. Smyrl, *Corrosion Science*, **42**(9), 1661-1668, 2000.
197. M. A. Jakab, D. A. Little, and J. R. Scully, *Journal of the Electrochemical Society*, **152**(8), 311-320, 2005.
198. M. A. Alodan, and W. H. Smyrl, *Journal of the Electrochemical Society*, **145**(5), 1571-1577, 1998.
199. N. Missert, R. G. Copeland, J. C. Barbour, J. E. Mikkalson, and H. Isaacs, *Proceedings - Electrochemical Society*, **2000-23**(Corrosion and Corrosion Prevention of Low Density Metals and Alloys), 239-246, 2001.
200. N. Missert, R. G. Copeland, Y. Kim, and R. Buchheit, Corrosion and Protection of Light Metal Alloys - Proceedings of the International Symposium, Oct 12-17 2003, Orlando, FL., United States, Electrochemical Society Inc., Pennington, United States, p. 55-61, 2003.
201. B. Mazurkiewicz, *Corrosion Science*, **23**(7), 687-691, 1983.
202. B. Mazurkiewicz, and A. Piotrowski, *Corrosion Science*, **23**(7), 697-701, 1983.
203. K. A. Yasakau, M. L. Zheludkevich, S. V. Lamaka, and M. G. S. Ferreira, *Journal of Physical Chemistry B*, **110**(11), 5515-5528, 2006.
204. G. O. Ilevbare, and J. R. Scully, *Corrosion (Houston, TX, United States)*, **57**(2), 134-152, 2001.
205. K. Sugimoto, K. Hoshino, M. Kageyama, S. Kageyama, and Y. Sawada, *Corrosion Science*, **15**(11-12), 709-720, 1975.
206. M. J. Pryor, and J. C. Fister, *Journal of the Electrochemical Society*, **131**(6), 1230-1235, 1984.
207. S. J. Ketcham, and F. H. Haynie, *Corrosion*, **19**(7), 242-246, 1963.
208. K. Nisancioglu, K. Y. Davanger, O. Strandmyr, and H. Holton, *Journal of the Electrochemical Society*, **128**(7), 1523-1526, 1981.
209. Y. Baek, and G. S. Frankel, *Journal of the Electrochemical Society*, **150**(1), B1-B9, 2003.
210. C. Blanc, B. Lavelle, and G. Mankowski, *Corrosion Science*, **39**(3), 495-510, 1997.
211. D. Zhu, and W. J. van Ooij, *Corrosion Science*, **45**(10), 2163-2175, 2003.
212. P. Campestrini, H. Terryn, A. Hovestad, and J. H. W. de Wit, *Surface & Coatings Technology*, **176**(3), 365-381, 2004.

213. M. L. Zheludkevich, K. A. Yasakau, S. K. Poznyak, and M. G. S. Ferreira, *Corrosion Science*, **47**(12), 3368-3383, 2005.
214. J. H. W. De Wit, *Electrochimica Acta*, **46**(24-25), 3641-3650, 2001.
215. A. Kolics, A. S. Besing, P. Baradlai, and A. Wieckowski, *Journal of the Electrochemical Society*, **150**(11), 512-516, 2003.
216. A. J. Aldykewicz, Jr., H. S. Isaacs, and A. J. Davenport, *Journal of the Electrochemical Society*, **142**(10), 3342-3350, 1995.
217. J. R. Scully, in *Encyclopedia of Electrochemistry: Corrosion and Oxide Films*, A. J. Bard and M. Stratmann (Editors), WILEY-VCH Verlag GmbH & Co. KGaA, Weinheim, p. 344-384, 2003.
218. A. Rota, and H. Boehni, *Materials Science Forum*, **44-45**(Electrochem. Methods Corros. Res.), 177-190, 1989.
219. A. Rota, and H. Boehni, *Werkstoffe und Korrosion*, **40**(4), 219-228, 1989.
220. A. Garner, and D. Tromans, *Corrosion*, **35**(2), 55-60, 1979.
221. B. W. Lifka, in *Corrosion Engineering Handbook*, P. A. Schweitzer (Editor), Marcel Dekker, Inc., NY, p. 99-155, 1996.
222. S. Maitra, and G. C. English, *Metallurgical Transactions A (Physical Metallurgy and Materials Science)*, **12A**(3), 535-541, 1981.
223. F. Andreatta, H. Terryn, and J. H. W. De Wit, *Electrochimica Acta*, **49**(17-18), 2851-2862, 2004.
224. P. Doig, P. E. J. Flewitt, and J. W. Edington, *Corrosion*, **33**(6), 217-221, 1977.
225. P. Doig, and J. W. Edington, *Nuclear Technology*, 461-476, 1975.
226. V. S. Sinyavskii, V. V. Ulanova, and V. D. Kalinin, *Protection of Metals (Translation of Zashchita Metallov)*, **40**(5), 481-490, 2004.
227. T. Ramgopal, P. I. Gouma, and G. S. Frankel, *Corrosion*, **58**(8), 687-697, 2002.
228. K. Urushino, and K. Sugimoto, *Corrosion Science*, **19**(4), 225-236, 1979.
229. M. Yasuda, F. Weinberg, and D. Tromans, *Journal of the Electrochemical Society*, **137**(12), 3716-3723, 1990.
230. B. Venkataraman, K. G. Rao, and M. Saletore, Science & Technology of Al-Li Alloys, HAL, Bangalore, p. 209-212, 1989.
231. Q. Zhang, F. B. Song, D. Li, and X. Y. Ding, *Materials Science Forum*, **396-402**(Pt. 3, Aluminium Alloys 2002), 1479-1484, 2002.
232. D. A. Little, B. J. Connolly, and J. R. Scully, *Corrosion Science*, **49**(2), 347-372, 2007.
233. W. Zhang, and G. S. Frankel, *Electrochemical and Solid-State Letters*, **3**(6), 268-270, 2000.
234. W. Zhang, S. Ruan, D. A. Wolfe, and G. S. Frankel, *Corrosion Science*, **45**(2), 353-370, 2003.
235. S. J. Fox, "*An In Situ X-ray Tomography Study of the Growth and Development of Localized Corrosion in Friction Stir Welded AA2024-T351*", University of Birmingham, MRes Thesis, 2007.
236. G. Kotsikos, J. M. Sutcliffe, and N. J. H. Holroyd, *Corrosion Science*, **42**(1), 17-33, 2000.
237. E. M. Gutman, *Mechanochemistry of Solid Surfaces*, World Scientific, Singapore, 1994.
238. E. M. Gutman, *Mechanochemistry of Materials*, Cambridge International Science Publishing, Cambridge, 1998.
239. P. L. Harrison, *Corrosion Science*, **7**(12), 789-794, 1967.

240. V. Vignal, R. Oltra, and N. Mary, Paper No. 04446, NACE, New Orleans, US, p., 2004.
241. X. Liu, and G. S. Frankel, *Corrosion Science*, **48**(10), 3309-3329, 2006.
242. V. S. Sinyavskii, and A. M. Semenov, *Protection of Metals (Translation of Zashchita Metallov)*, **38**(2), 132-140, 2002.
243. O. Lunder, B. Olsen, and K. Nisancioglu, *International Journal of Adhesion and Adhesives*, **22**(2), 143-150, 2002.
244. L. Kozma, and I. Olefjord, *Materials Science and Technology*, **3**(10), 860-874, 1987.
245. P. Campestrini, E. P. M. Van Westing, and J. H. W. De Wit, *Electrochimica Acta*, **46**(16), 2553-2571, 2001.
246. A. Afseth, J. H. Nordlien, G. M. Scamans, and K. Nisancioglu, *Corrosion Science*, **44**(11), 2543-2559, 2002.
247. A. Afseth, J. H. Nordlien, G. M. Scamans, and K. Nisancioglu, *Corrosion Science*, **44**(11), 2491-2506, 2002.
248. K. Nisancioglu, J. H. Nordlien, A. Afseth, and G. M. Scamans, Charlottesville, VA, USA, Trans Tech Publications, p. 111-126, 2000.
249. O. Lunder, K. F. Heen, and K. Nisancioglu, *Corrosion*, **60**(7), 622-631, 2004.
250. G. S. Frankel, and R. L. McCreery, *Electrochemical Society Interface*, **10**(4), 34-38, 2001.
251. K. Nisancioglu, O. Lunder, and H. Holtan, *Corrosion*, **41**(5), 247-257, 1985.
252. O. Lunder, and K. Nisancioglu, *Corrosion*, **44**(7), 414-422, 1988.
253. C. E. Moffitt, D. M. Wieliczka, and H. K. Yasuda, *Surface and Coating Technology*, **137**, 188-196, 2001.
254. R. Pinner, and S. Wernick, *The Surface Treatment and Finishing of Aluminium and its Alloys*, Robert Draper Ltd., Teddington, 1972.
255. E. V. Koroleva, G. E. Thompson, G. Hollrigl, and M. Bloeck, *Corrosion Science*, **41**(8), 1475-1495, 1999.
256. A. E. Hughes, G. Theodossiou, S. Elliott, T. G. Harvey, P. R. Miller, J. D. Gorman, and J. K. Paterson, *Materials Science and Technology*, **17**, 1642-1652, 2001.
257. A. J. Davenport, and B. Liu, Corrosion and Corrosion Prevention of Low Density Metals and Alloys, The Electrochemical Society, p. 41-46, 2001.
258. A. J. Davenport, F. A. M. Moulinier, B. Liu, and P. C. Morgan, Aluminium Surface Science and Technology, Manchester, UK, p., 2000.
259. K. J. H. Nelson, A. E. Hughes, R. J. Taylor, B. R. W. Hinton, L. Wilson, and M. Henderson, *Materials Science and Technology*, **17**, 1211-1221, 2001.
260. A. E. Hughes, K. J. H. Nelson, and P. R. Miller, *Materials Science and Technology*, **15**, 1124-1132, 1999.
261. E. Maire, J. Y. Buffiere, L. Salvo, J. J. Blandin, W. Ludwig, and J. M. Letang, *Advanced Engineering Materials*, **3**(8), 539-546, 2001.
262. M. Stampanoni, G. Borchert, P. Wyss, R. Abela, B. Patterson, S. Hunt, D. Vermeulen, and P. Ruegsegger, *Nuclear Instruments and Methods in Physics Research, Section A: Accelerators, Spectrometers, Detectors and Associated Equipment*, **491**(1-2), 291-301, 2002.
263. M. Stampanoni, R. Abela, G. Borchert, and B. D. Patterson, Developments in X-Ray Tomography IV, Aug 4-6 2004, Denver, CO, United States, International Society for Optical Engineering, Bellingham, WA 98227-0010, United States, p. 169-181, 2004.

264. B. D. Patterson, R. Abela, H. Auderset, Q. Chen, F. Fauth, F. Gozzo, G. Ingold, H. Kuhne, M. Lange, D. Maden, D. Meister, P. Pattison, T. Schmidt, B. Schmitt, C. Schulze-Briese, M. Shi, M. Stampanoni, and P. R. Willmott, *Nuclear Instruments and Methods in Physics Research, Section A: Accelerators, Spectrometers, Detectors and Associated Equipment*, **540**(1), 42-67, 2005.
265. M. Stampanoni, P. Wyss, R. Abela, G. Borchert, D. Vermeulen, and P. Ruegsegger, Developments in X-Ray Tomography III, Aug 2-3 2001, San Diego, CA, United States, The International Society for Optical Engineering, p. 42-53, 2001.
266. L. Salvo, P. Cloetens, E. Maire, S. Zabler, J. J. Blandin, J. Y. Buffiere, W. Ludwig, E. Boller, D. Bellet, and C. Josserond, *Nuclear Instruments and Methods in Physics Research, Section B: Beam Interactions with Materials and Atoms*, **200**(SUPPL), 273-286, 2003.
267. S. R. Stock, *International Materials Reviews*, **44**(4), 141-164, 1999.
268. E. Maire, J. Y. Buffiere, R. Mokso, P. Cloetens, and W. Ludwig, *Materials Science Forum*, **519-521**, 1367-1372, 2006.
269. G. N. Hounsfield, *British Journal of Radiology*, **46**(552), 1016-1022, 1973.
270. G. Peix, N. Duvauchelle, and N. Freud, in *X-Ray Tomography in Material Science*, J. Baruchel, J. Y. Buffiere, E. Maire, P. Merle and G. Peix (Editors), Hermes Science, Paris, p. 15-27, 2000.
271. C. R. Coutant, and A. Marc, in *X-Ray Tomography in Material Science*, J. Baruchel, J. Y. Buffiere, E. Maire, P. Merle and G. Peix (Editors), Hermes Science, Paris, p. 61-75, 2000.
272. L. Salvo, P. Cloetens, E. Maire, S. Zabler, J. J. Bladin, J. Y. Buffiere, W. Ludwig, E. Boller, D. Bellet, and C. Josserond, *Nuclear Instruments & Methods in Physics Research B*, **200**, 273-286, 2003.
273. J. Baruchel, E. Boller, P. Cloetens, W. Ludwig, and F. Peyrin, in *X-Ray Tomography in Material Science*, J. Baruchel, J. Y. Buffiere, E. Maire, P. Merle and G. Peix (Editors), Hermes Science, Paris, p. 29-43, 2000.
274. L. Babout, W. Ludwig, E. Maire, and J. Y. Buffiere, *Nuclear Instruments and Methods in Physics Research, Section B: Beam Interactions with Materials and Atoms*, **200**(SUPPL), 303-307, 2003.
275. J.-Y. Buffiere, E. Maire, P. Cloetens, G. Lormand, and R. Fougeres, *Acta Materialia*, **47**(5), 1613-1625, 1999.
276. L. Babout, E. Maire, J. Y. Buffiere, and R. Fougeres, *Acta Materialia*, **49**(11), 2055-2063, 2001.
277. E. Maire, J. C. Grenier, and L. Babout, *Materials Science Forum*, **519-521**, 821-827, 2006.
278. E. Maire, and J. Y. Buffiere, in *X-Ray Tomography in Material Science*, J. Baruchel, J. Y. Buffiere, E. Maire, P. Merle and G. Peix (Editors), Hermes Science Publications, Paris, p. 115-125, 2000.
279. E. Maire, L. Babout, J. Y. Buffiere, and R. Fougeres, *Materials Science & Engineering A (Structural Materials: Properties, Microstructure and Processing)*, **A319-321**, 216-219, 2001.
280. D. Bernard, G. L. Vignoles, and J. M. Heintz, in *X-Ray Tomography in Material Science*, J. Baruchel, J. Y. Buffiere, E. Maire, P. Merle and G. Peix (Editors), Hermes Science Publications, Paris, p. 177-191, 2000.
281. T. J. Marrow, J.-Y. Buffiere, P. J. Withers, G. Johnson, and D. Engelberg, *International Journal of Fatigue*, **26**(7), 717-725, 2004.

282. T. J. Marrow, H. Cetinel, M. Al-Zalmah, S. Macdonald, P. J. Withers, and J. Walton, *Fatigue and Fracture of Engineering Materials and Structures*, **25**(7), 635-648, 2002.
283. K. H. Khor, J.-Y. Buffiere, W. Ludwig, H. Toda, H. S. Ubhi, P. J. Gregson, and I. Sinclair, *Journal of Physics Condensed Matter: Synchroton Radiation for Advanced Materials Analysis and Processing*, **16**(33), 3511-3515, 2004.
284. H. Toda, I. Sinclair, J.-Y. Buffiere, E. Maire, T. Connolley, M. Joyce, K. H. Khor, and P. Gregson, *Philosophical Magazine*, **83**(21), 2429-2448, 2003.
285. A. Guvenilir, T. M. Breunig, J. H. Kinney, and S. R. Stock, *Acta Materialia*, **45**(5), 1977-1987, 1997.
286. A. Guvenilir, and S. R. Stock, *Fatigue and Fracture of Engineering Materials & Structures*, **21**(4), 439-450, 1998.
287. T. J. Marrow, L. Babout, A. P. Jivkov, P. Wood, D. Engelberg, N. Stevens, P. J. Withers, and R. C. Newman, *Journal of Nuclear Materials*, **352**(1-3), 62-74, 2006.
288. B. J. Connolly, D. A. Homer, S. J. Fox, A. J. Davenport, C. Padovani, S. Zhou, A. Turnbull, M. Preuss, N. P. Stevens, T. J. Marrow, J. Y. Buffiere, E. Boller, A. Groso, and M. Stampanoni, *Materials Science and Technology*, **22**(9), 1076-1085, 2006.
289. A. J. Davenport, C. Padovani, B. J. Connolly, N. P. C. Stevens, T. A. W. Beale, A. Groso, and M. Stampanoni, *Electrochemical and Solid-State Letters*, **10**(2), 5-8, 2007.
290. L. Babout, T. J. Marrow, D. Engelberg, and P. J. Withers, *Materials Science and Technology*, **22**(9), 1068-1075, 2006.
291. G. Y. Baaklini, R. T. Bhatt, A. J. Eckel, P. Engler, M. G. Castelli, and R. W. Rauser, *Materials Evaluation*, **53**(9), 1040-1044, 1995.
292. J. H. Kinney, S. R. Stock, M. C. Nichols, U. Bonse, T. M. Breunig, R. A. Saroyan, R. Nusshardt, Q. C. Johnson, F. Busch, and S. D. Antolovich, *Journal of Materials Research*, **5**(5), 1123-1129, 1990.
293. R. N. Yancey, and G. Y. Baaklini, *Journal of Engineering for Gas Turbines and Power, Transactions of the ASME*, **116**(3), 635-639, 1994.
294. S. R. Stock, L. L. Dollar, G. B. Freeman, W. J. Ready, L. J. Turbini, J. C. Elliott, P. Anderson, and G. R. Davis, Proceedings of the Fall 1993 MRS Meeting, Nov 29-Dec 3 1993, Boston, MA, USA, Publ by Materials Research Society, Pittsburgh, PA, USA, p. 65-69, 1994.
295. L. L. Dollar, "*Evaluation of nondestructive x-ray techniques for electronic packaging materials*", Georgia Institute of Technology, MS Thesis, 1992.
296. C. F. Martin, C. Josserond, L. Salvo, J. J. Blandin, P. Cloetens, and E. Boller, *Scripta Materialia*, **42**(4), 375-381, 2000.
297. A. Elmoutaouakkil, L. Salvo, E. Maire, and G. Peix, *Advanced Engineering Materials*, **4**(10), 803-807, 2002.
298. P. Cloetens, W. Ludwig, D. Van Dyck, J. P. Guigay, M. Schlenker, and J. Baruchel, *Proceedings of SPIE - The International Society for Optical Engineering; Proceedings of the 1999 Developments in X-Ray Tomography II, Jul 22-Jul 23 1999*, **3772**, 279-290, 1999.
299. P. Cloetens, W. Ludwig, J. Baruchel, D. Van Dyck, J. Van Landuyt, J. P. Guigay, and M. Schlenker, *Applied Physics Letters*, **75**(19), 2912-2914, 1999.
300. W. Ludwig, and D. Bellet, *Materials Science and Engineering A: Structural Materials: Properties, Microstructure and Processing*, **281**(1), 198-203, 2000.

301. W. Ludwig, J.-Y. Buffiere, S. Savelli, and P. Cloetens, *Acta Materialia*, **51**(3), 585-598, 2003.
302. R. J.-P. Doyle, "*The Effect of Welding Parameters, Laser Surface Melting Techniques and Shot Peening on the Corrosion Behaviour and Fatigue Properties of Friction Stir Welded AA2024-T351*", University of Birmingham, Masters of Research Thesis, 2006.
303. D. R. Lide, *CRC Handbook of Chemistry and Physics*, CRC Press, Online Edition, 2000.
304. K. S. Ferrer, and R. G. Kelly, *Corrosion*, **57**(2), 110-117, 2001.
305. T. Suter, and H. Bohni, *Electrochimica Acta*, **43**(19-20), 2843-2849, 1998.
306. T. Suter, Y. Mueller, P. Schmutz, and O. von Trzebiatowski, *Advanced Engineering Materials*, **7**(5), 339-348, 2005.
307. M. M. Lohrengel, A. Moehring, and M. Pilaski, *Electrochimica Acta*, **47**(1-2), 137-141, 2001.
308. M. M. Lohrengel, C. Rosenkranz, I. Kluppel, A. Moehring, H. Bettermann, B. V. d. Bossche, and J. Deconinck, *Electrochimica Acta*, **49**(17-18), 2863-2870, 2004.
309. N. Birbilis, B. N. Padgett, and R. G. Buchheit, *Electrochimica Acta*, **50**(16-17), 3536-3544, 2005.
310. N. Mary, V. Vignal, R. Oltra, and L. Coudreuse, *Journal of Materials Research*, **19**(12), 3688-3694, 2004.
311. C. Padovani, "*Corrosion Protection of Friction Stir Welds in Aerospace Aluminium Alloys*", University of Birmingham, PhD Thesis, 2007.
312. J. F. Nye, *Physical Properties of Crystals: Their Representation by Tensors and Matrices*, Oxford University Press, Oxford, 1985.
313. M. Jariyaboon, A. J. Davenport, R. Ambat, B. J. Connolly, S. W. Williams, and D. A. Price, *Corrosion Science*, **49**(2), 877-909, 2007.
314. L. A. Feldkamp, L. C. Davis, and J. W. Kress, *Journal of the Optical Society of America A (Optics and Image Science)*, **1**(6), 612-619, 1984.
315. C. Blanc, B. Lavelle, and G. Mankowski, *Materials Science Forum*, **217-222**(3), 1559-1564, 1996.
316. S. Hoerle, B. Malki, and B. Baroux, *Journal of the Electrochemical Society*, **153**(12), B527-B532, 2006.
317. C. Blanc, A. Freulon, M.-C. Lafont, Y. Kihn, and G. Mankowski, *Corrosion Science*, **48**(11), 3838-3851, 2006.
318. K. R. Trethewey, and J. Chamberlain, *Corrosion for Science and Engineering*, Addison Wesley Longman Limited, Essex, UK, 1998.
319. X. Liu, G. S. Frankel, B. Zoofan, and S. I. Rokhlin, *Journal of the Electrochemical Society*, **153**(2), 42-51, 2006.
320. W. Zhang, and G. S. Frankel, *Journal of the Electrochemical Society*, **149**(11), B510-B519, 2002.
321. C. Augustin, E. Andrieu, C. Blanc, G. Mankowski, and J. Delfosse, *Journal of the Electrochemical Society*, **154**(11), C637-C644, 2007.
322. R. H. Jones, M. A. Friesel, and R. Pathania, *Corrosion (Houston)*, **47**(2), 105-115, 1991.
323. T. Suter, E. G. Webb, H. Bohni, and R. C. Alkire, Chemistry and Electrochemistry of Corrosion and Stress Corrosion Cracking, New Orleans, LA, p. 301-317, 2001.
324. T. K. Christman, *Corrosion (Houston)*, **46**(6), 450-453, 1990.

325. T. P. Hoar, D. C. Mears, and G. P. Rothwell, *Corrosion Science*, **5**(4), 279-289, 1965.
326. G. T. Burstein, and S. P. Mattin, Critical Factors in Localized Corrosion II, Chicago, IL, USA, Electrochem. Soc, p. 1-14, 1996.
327. S. P. Mattin, and G. T. Burstein, *Philosophical Magazine Letters*, **76**(5), 341-347, 1997.
328. T. P. Hoar, *Corrosion Science*, **7**(6), 341-355, 1967.